Narantsetseg et al, 2021. Mongolian Geoscientist 26 (52) 16-45
DOI: https://doi.org/10.5564/mgs.v26i52.1079

Mongolian Geoscientist

Original article

Metamorphic rocks from the north-eastern part of the Ereendavaa terrane (Eastern Mongolia): an origin of the Permian back-arc basin rather than the Proterozoic basement

Tserendash Narantsetseg[1*], Yuan Chao[2], Wang Tao[3], Ren Zhongyuan[2], Li Pengfei[2], Zhang Le[2], Guo Lei[3], Tong Ying[3], Demberel Orolmaa[1], Altanbaatar Battushig[4], Orosoo Baatarchuluun[5], Tuya Idermunkh[5], Jargalsaikhan Tumendelger[5]

[1]*Department of Regional Geology and Tectonics, Institute of Geology, Mongolian Academy of Sciences, Ulaanbaatar 15160, Mongolia*
[2]*Guangzhou Institute of Geochemistry, Chinese Academy of Sciences, Guangzhou, 510640, China*
[3]*Institute of Geology, Chinese Academy of Geological Sciences, 100037 Beijing, China*
[4]*National Geological Survey of Mongolia, Ulaanbaatar 18072, Mongolia*
[5]*Ikh-Tsog Undur LLC, Ulaanbaatar 15160, Mongolia*

**Corresponding author: ts_narangeo@yahoo.com, ORCID: 0000-0001-5402-1147*

ARTICLE INFO

Article history:
Received 28 March, 2021
Accepted 19 June, 2021

ABSTRACT

In this paper, we have conducted geochronological and geochemical studies on the metamorphic rocks of the Khaychingol and Ereendavaa Formations in the Mogoitiin Gol, Khaychin Gol and Emgentiin Bulag areas from the Ereendavaa terrane and these rocks have been considered to be Precambrian in age. However, new LA–ICP–MS zircon U–Pb dating results indicate that the protolith of the studied metamorphic rocks was formed in two stages: 1) during ~ 296 - 285 Ma, the protolith of mafic, felsic and black schists formed; 2) during ~276 - 271 Ma, the protolith of gneiss and psammitic schists began to deposit. The Early Permian bimodal association composed of low-K basalt and comagmatic high-Na, low-K dacite with high-K calc-alkaline rhyolite, represent protolith of the mafic and felsic schists which were formed in back-arc basin environment. The Middle Permian gneiss, and psammitic schists with sedimentary protolith have geochemical signatures of island arc rocks, such as enrichment of LILE relative to HFSE, and markedly negative Nb, Ta and Ti anomalies, suggesting that they were formed in a continental arc environment. Considering a close spatial relationship of the Ereendavaa terrane with the Mongol-Okhotsk Belt in the north-west, we propose that accompanied with the emplacement of arc magmatic rocks, the arc rifting occurred and formed the Early Permian bimodal volcanic rocks. In the Late Permian, after the formation of the back-arc basin, deposition of the immature deposits as wacke, arkose and litharenite dominated sediments in a continental arc environment started.

Keywords: Khaychingol and Ereendavaa Formation, high-Na dacite, geochronology, geochemistry

INTRODUCTION

Mongolia lies in the central part of the Central Asian Orogenic Belt (Mossakovsky et al., 1994; Zorin, 1999; Badarch et al., 2002; Khain et al., 2003; Jahn, 2004; Windley et al., 2007; Xiao et al, 2010), or Altaids (Sengör et al., 1993; Sengör and Natal'in, 1996), which is fringed by the Siberian Craton in the north and the Tarim and Sino-Korean (North China) Cratons in the south (Fig. 1a), and contains several continental massifs/blocks that are separated by fold belts (Tomurtogoo, 2014). The Kherlen massif

situated in the North-Eastern Mongolia consists, from north to south, of the Ereendavaa, Undur-Khaan (Herlen terrane after Badarch et al., 2002) and Idermeg terranes, all extending in NE -SW direction (Badarch et al., 2002; Tomurtogoo, 2002). The Ereendavaa terrane is one of the constituent terranes of Kherlen Massif (Fig. 1b), which represents the Mongolian part of the Argun-Idermeg superterrane (Parfenov et al., 2009; Kotov et al., 2013) or so called Central Mongolia-Erguna Belt (Wang et al., 2017). The terrane is bordered by the Mongol-Okhotsk Orogenic Belt to the northeast (by Mongol-Okhotsk suture) and by the Idermeg and Undurkhaan terranes (by Kherlen suture) to the south and southeast (Tomurtogoo, 2002).

It is widely accepted that the Paleozoic tectonic evolution of the Ereendavaa terrane was dominated by the amalgamation of microcontinental massifs and closure of the Paleo-Asian Ocean, while the Mesozoic evolution was largely influenced by the Mongol -Okhotsk tectonic systems (Dash et al., 2015; Wang et al., 2015; Miao et al., 2016; 2017; 2020; Narantsetseg et al., 2019; Sheldrick et al., 2020).

The Ereendavaa terrane was previously classified as a cratonic terrane (Badarch et al., 2002), but it was later defined as an active continental margin (Tomurtogoo, 2002; 2012, 2014) with Paleoproterozoic to Mesoproterozoic basement and Neoproterozoic metasedimentary and volcanic rocks. The metamorphic rocks of the Khaychingol and Ereendavaa Formation scattered in the Ereendavaa terrane, have long been interpreted to represent the Precambrian basement (Marinov et al., 1973; Blagonravov et al., 1990; Dorjnamjaa and Bat-Ireedui, 1991; Baymba, 1991; Dorjnamjaa et al., 2012; Tomurtogoo, 2012; Tomurtogoo, 2014; Erdenechimeg et al., 2017). However, recent studies show that various schist, gneiss and amphibolite from the north-eastern part of the Ereendavaa terrane mainly have protolith ages from Paleozoic to Mesozoic rather than Precambrian (Daoudene et al., 2009; 2013; Miao et al., 2017). In contrast, Late

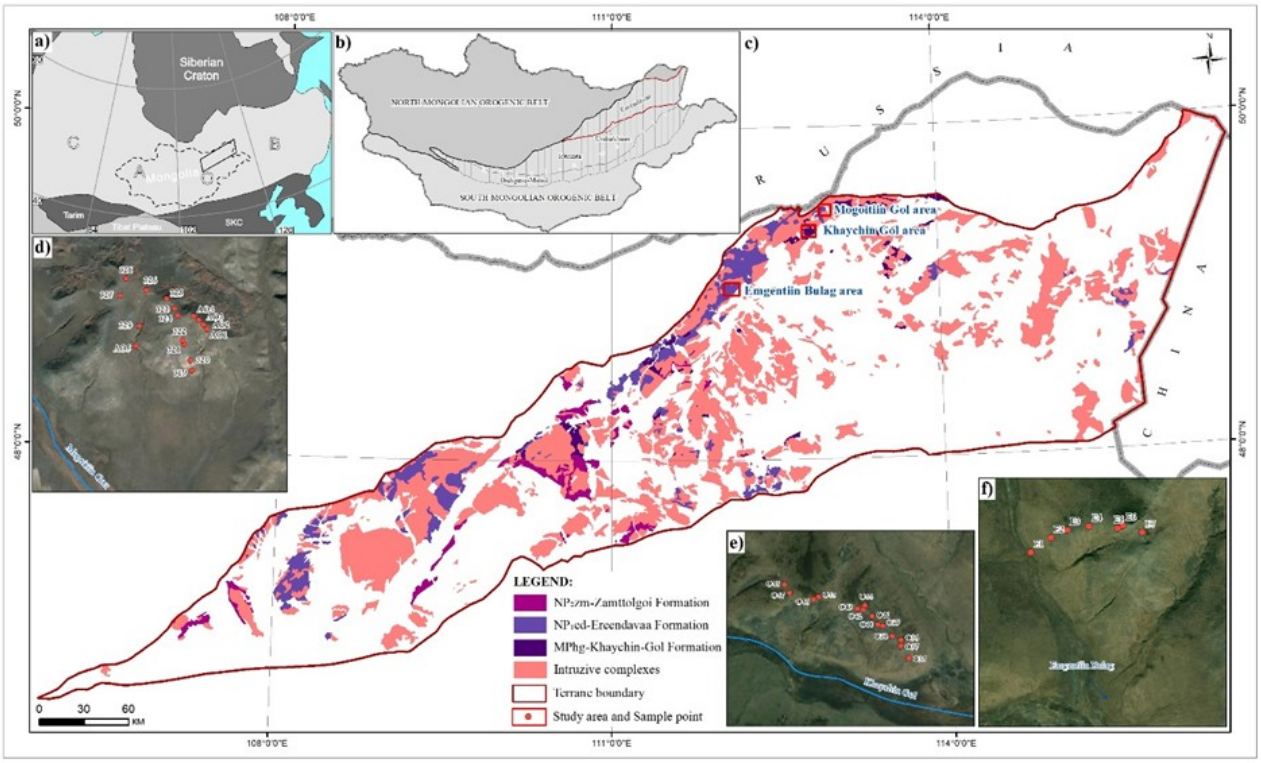

Fig. 1. a) Relationship of the study area with the Central Asian Orogenic Belt; b) Simplified tectonic zoning of fold areas in Mongolia (modified after Tomurtogoo, 2014); c) Simplified geological map of the Ereendavaa terrane (after Geology map of Mongolia with scale of 1:500000). Inset (d, e and f) shows sampling sites of each study areas.

Mesoproterozoic (ca. 1.2–1.15 Ga; Miao et al., 2020) and Late Neoproterozoic (ca. 550 and 630 Ma; Narantsetseg et al., 2015; 2018) ages were obtained from the south-western part of the terrane.

However, the possibility of presence of Precambrian rocks within the north-eastern part of the terrane still not excluded. Therefore, our study focused on the Mogoitiin Gol, Khaychin Gol and Emgentiin Bulag areas which were considered to be key areas in having Precambrian rocks. This study reports integrated petrography, whole-rock geochemistry and LA-ICP-MS zircon U-Pb ages of metamorphic rocks

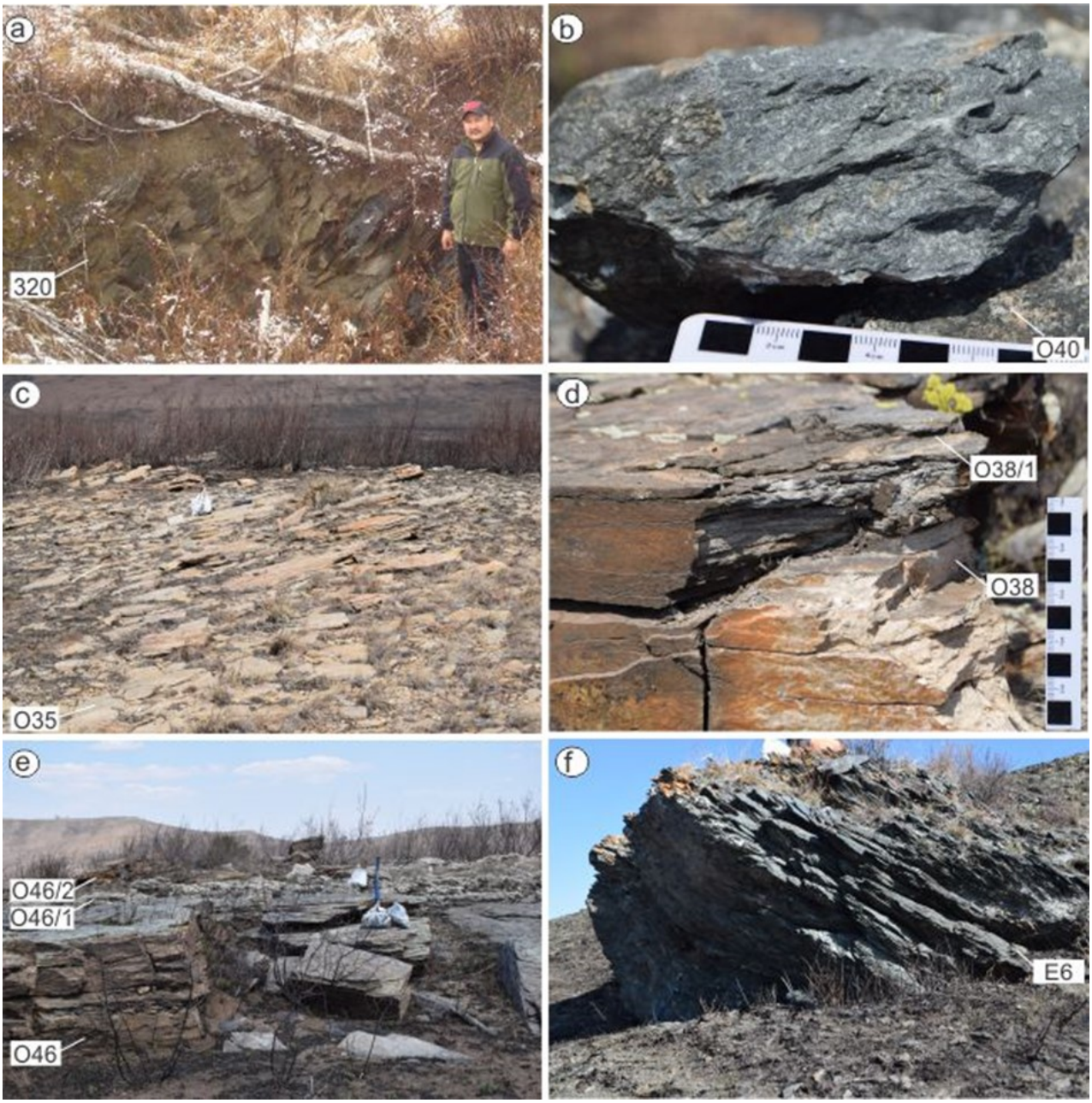

Fig. 2. Field photos of the typical metamorphic rocks of the Khaychingol and Ereendavaa Formations**.** a) Outcrops of black schist from Mogoitiin Gol area (sample 320). b) Hornblende schist (sample O40), c) Biotite-plagioclase gneiss (sample O35), d) Biotite-plagioclase gneiss (sample O38) and biotite-quartz-plagioclase schist (sample O38/1), and e) Two-mica quartz schist (sample O46), muscovite schist (sample O46/1) and biotite-plagioclase gneiss (sample O46/1) from Khaychin Gol area. f) Quartz-chlorite schist (sample E6) from Emgentiin Bulag area

from the Khaychingol and Ereendavaa Formation in the north-eastern part of the Ereendavaa terrane.

GEOLOGICAL SETTING AND STRATIGRAPHIC SEQUENCES

The Ereendavaa terrane contains metamorphic rocks of Paleoproterozoic and Mesoproterozoic Khaychingol and Ereendavaa Formation overlying by Late Neoproterozoic-Early Cambrian terrigenous-carbonate and volcano-terrigenous formations, which were intruded by Upper Neoproterozoic to Mesozoic granitoid plutons (Fig. 1c).

The Khaychingol Formation mainly exposed as sparse small blocks in the south-eastern and north-eastern part of the Ereendavaa terrane, especially the Ikh Khaychin Gol, Baga Khaychin Gol, Bituu Gol and Mogoitiin Gol areas. The Khaychingol Formation consists of gneiss, quartz-biotite schist, hornblende schist, two-mica schist, chlorite-sericite schist and minor amphibolite and marble, with an overall thickness of 1200 – 1500 m. The Ereendavaa Formation is mainly distributed in the Nomon Gol, Nariin Gol, Zurug Gol, Onon Gol, Ulaan Zoogiin Bulag and Emgentiin Bulag areas and consists of black schist interlayered with thin metaconglomerate, metasandstone, metasiltstone and crystalline limestone in lower part and quartz-sericite, quartz-chlorite-sericite, sericite-chlorite and quartz-chlorite-carbonate-amphibole schists and minor calcareous sandstone and crystalline limestone in upper part. Total thickness is estimated about to be 3000 m (Blagonravov et al., 1990; Dorjnamjaa

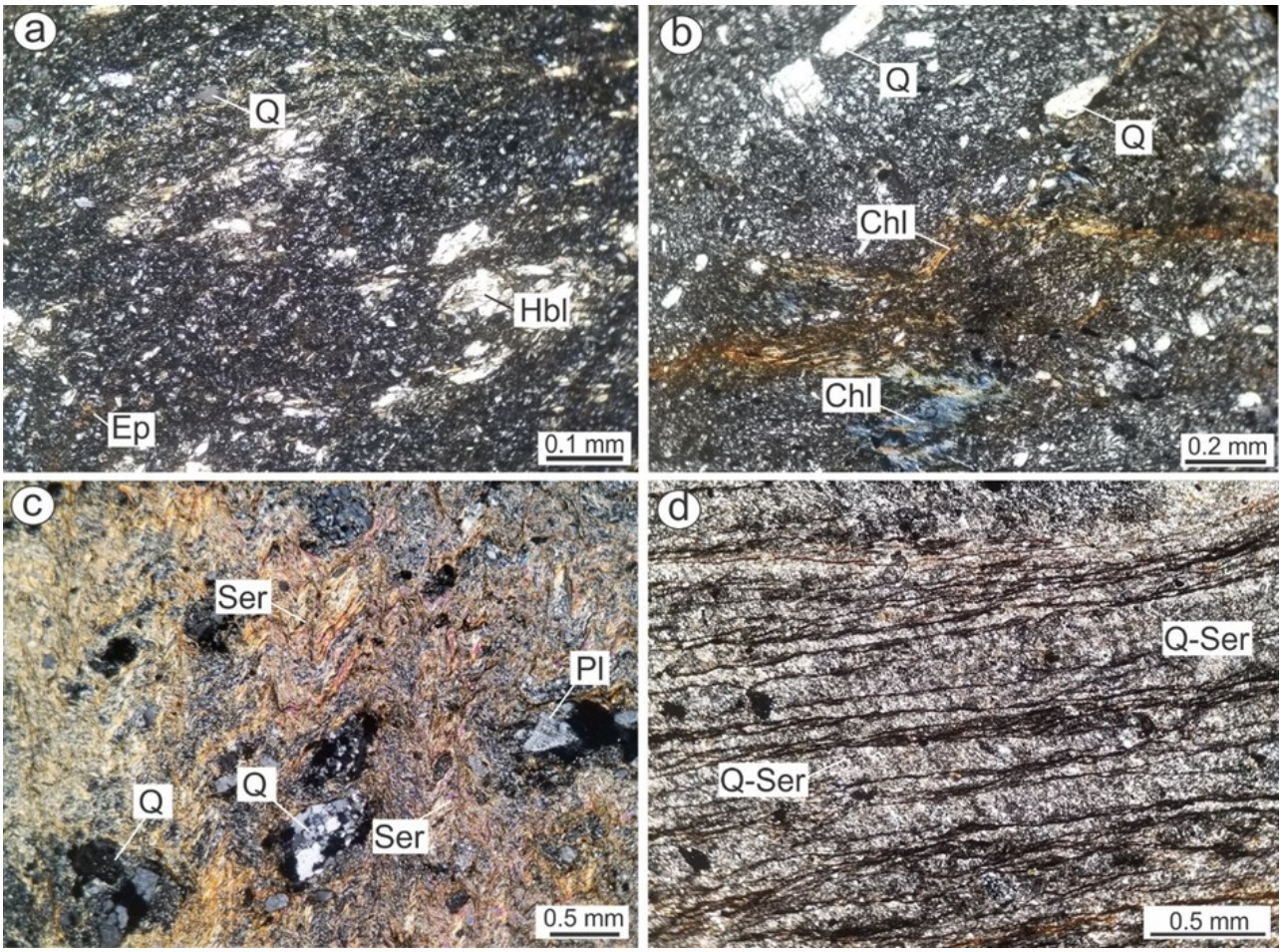

Fig. 3. Representative microphotographs of metamorphic rocks from the Mogoitiin Gol area. a) Hornblende schist (sample AO1), b) Chlorite-quartz schist (sample 324/1), c) Quartz-sericite schist (sample 323), d) Black schists (sample 320). Abbreviations: Q – quartz, Pl – plagioclase, Hbl – hornblende, Ep – epidote, Chl – chlorite, Ser – sericite. All photomicrographs are under cross-polarized light.

and Bat-Ireedui, 1991). The Khaychingol Formation shows mainly fault contact with the Ereendavaa Formation.

Stratigraphic sequence and petrography

During the field trip, we collected 32 typical gneiss and schists samples in the Khaychingol and Ereendavaa Formation from the Mogoitiin Gol, Khaychin Gol and Emgentiin Bulag areas, north-eastern part of the Ereendavaa terrane. The sampling sites are shown in Fig.1d, e and f and samples are described in the following paragraphs.

Mogoitiin Gol area

The Proterozoic sequences in the Mogoitiin Gol area are commonly referred to Ereendavaa Formation with Mesoproterozoic (Blagonravov et al., 1968; Dorjnamjaa and Batireedui, 1991; Dorjnamjaa et al., 2012) or Neoproterozoic (Erdenechimeg et al., 2017) ages. The studied section is located in the north-eastern part of the Mogoitiin Gol River (49^o 29’ 37.2’’; 112^o 55’ 50.2’’). The Ereendavaa Formation in this area mainly comprises yellowish, light-gray quartz-sericite schist, ash-gray chlorite-quartz schist, black schist (Fig. 2a) and minor dark greenish hornblende schist. Total thickness of studied section is 800 m.

Hornblende schist (sample AO1) is fine- to medium grained (sample O40, O42) and microlepidoblastic in texture. The rock is composed of amphibole (Hbl, 70 - 75 %), plagioclase (Pl, 10 - 15%), with minor amounts of quartz, epidote, carbonate and opaque mineral. The schistosity is represented by sub-oriented hornblende grains and plagioclase (Fig. 3a). The typical mineral assemblage is Hbl+Pl+Q, and its protolith interpreted to be mafic volcanic rock.

Chlorite-quartz schist (samples 324/1, 329). The chlorite-quartz schists mainly exhibit porphyroclastic texture with porphyroclasts (15 - 40% by volume) of broken plagioclase, quartz and minor alkali feldspar grains scattered in the fine grained foliated felsitic groundmass, same as a quartz-sericite schist. The rock is strongly deformed, and schistosity is defined by aligned chlorite flakes and quartz grains with preferred orientation (Fig. 3b). Its protolith was interpreted to be felsic volcanic rock.

Quartz-sericite schist (samples 319, 321, 321/1, 322, 323, 324, AO2, AO3, AO5). The quartz-sericite schists mainly exhibit porphyroclastic texture with porphyroclasts (5 – 45% by volume) of broken plagioclase, quartz and minor alkali feldspar grains scattered in the fine grained foliated felsitic groundmass (Fig. 3c). The schists were strongly deformed, and schistosity is well defined by aligned and crenulated sericite flakes, and sometimes sericite grains are poikiloblastic, with inclusions of quartz which were recrystallized to a granular mosaic. Its protolith was interpreted to be felsic volcanic rock.

Black schists (sample 320) are composed of thin laminated fine grained quartz-sericite aggregates (50 – 55%) and black colored clayey layers (40 - 45%) and contains minor opaque mineral and accessory zircon. In some case, biotite aggregates are associated with clayey layers (sample AO4) (Fig. 3d). Its protolith was interpreted to be sedimentary rocks.

Khaychin Gol area

The Proterozoic sequences in the Khaychin Gol area are referred to the Kaychingol Formation with Paleoproterozoic (Blagonravov et al., 1968; Dorjnamjaa and Batireedui, 1991; Dorjnamjaa et al., 2012) or Mesoproterozoic (Erdenechimeg et al., 2017) ages. The studied section is located in the north-eastern part of the Western Khaychin Gol (49^o 22’ 59.4’’; 112^o 51’ 0.2’’). The Khaychingol Formation in this area mainly comprises a sequence of yellowish gray garnet, rare tourmaline bearing biotite-plagioclase gneiss, light to grey mica schist and minor dark-green hornblende schist with different thicknesses (Fig. 2b-e). Total thickness of the studied section is 1000 m.

Hornblende schist generally fine- to medium grained (sample O40, O42) and lepidogranoblastic in texture. Mineral assemblage is variable and consists of mainly yellowish-green hornblende (Hbl, 60 – 85%) and plagioclase (Pl, 15 – 30%), *clinopyroxene (*Cpx*, 10 - 15%, only in sample O40 occur as relics)* with minor amount of quartz and opaque minerals (Fig. 4a). The schistosity is well defined by oriented hornblende (1 – 2 mm)

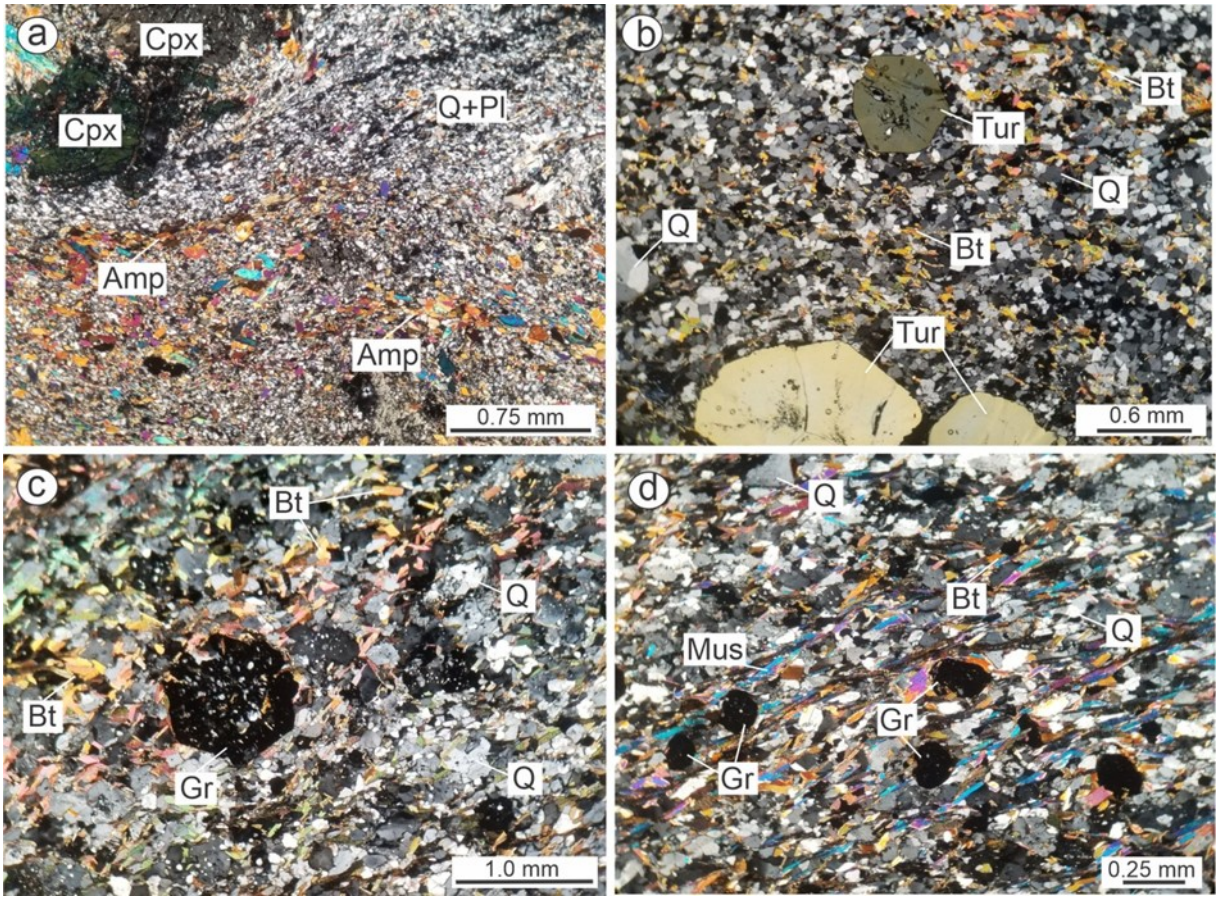

Fig. 4. Representative microphotographs of metamorphic rocks from the Khaychin Gol area. a) Hornblende schist (sample O40), b) Biotite-plagioclase gneiss (sample O42/1), c) Biotite-quartz-plagioclase schist (sample O38/1), d) Two-mica quartz schist (sampe O37/3), Abbreviations: Q – quartz, Pl – plagioclase, Amp – amphibole, Tur – tourmaline, Gr – garnet, Bt – biotite, Mus – muscovite. All photomicrographs are under cross-polarized light.

grains alternating with plagioclase and quartz aggregates. The nature of the protolith is interpreted to be mafic.

Biotite-plagioclase gneiss (samples O35, O36, O37, O38, O42/1) is fine to medium grained and consists of recrystallized quartz grains (Q, 60 – 65 %) with serrated margins, plagioclase (Pl, 15 – 20%), biotite (Bt, 5 - 10 %) and trace amounts of garnet (Grt), tourmaline (Tur) and opaque minerals (Fig. 4b). The rock is slightly foliated, defined by aligned biotite grains. The biotite is generally subidiomorphic and occur at grain boundaries and ranges from 0.5 to 1 mm in length. Quartz together with plagioclase ranges from 0.1 to 2.0 mm in size. Tourmaline is euhedral and 0.6 to 2.4 mm in diameter. Garnet is euhedral to subhedral, and to 2.2 mm in size. The typical mineral assemblage is Grt+Bt+Pl+Qtz+Tur. The gneiss was deformed, with the polycrystalline quarts. Its protolith is interpreted to be sedimentary rocks.

There are three main types of the **mica schists**: plagioclase-biotite-quartz schist, two-mica quartz schist and quartz-muscovite schist. All these schists are fine to medium grained and strongly foliated. Their foliation is represented by parallel flakes of mica. Biotite-quartz-plagioclase schist (samples O37/2, O38/1, O43, O45) is composed of quartz (Q, 20 - 25%), biotite (Bt, 25 - 40%), plagioclase (Pl, 30 - 35%), with trace amount of garnet (Grt) grains (Fig. 4c). Two-mica quartz schist (samples O37/3, O46, O47/1) is composed of mainly quartz (Q, 50 - 60%), biotite (Bt, 15 - 20%), muscovite (Mus, 5 - 10%) and plagioclase (Pl, 15 - 20%) and rare garnet (Grt) grains. The

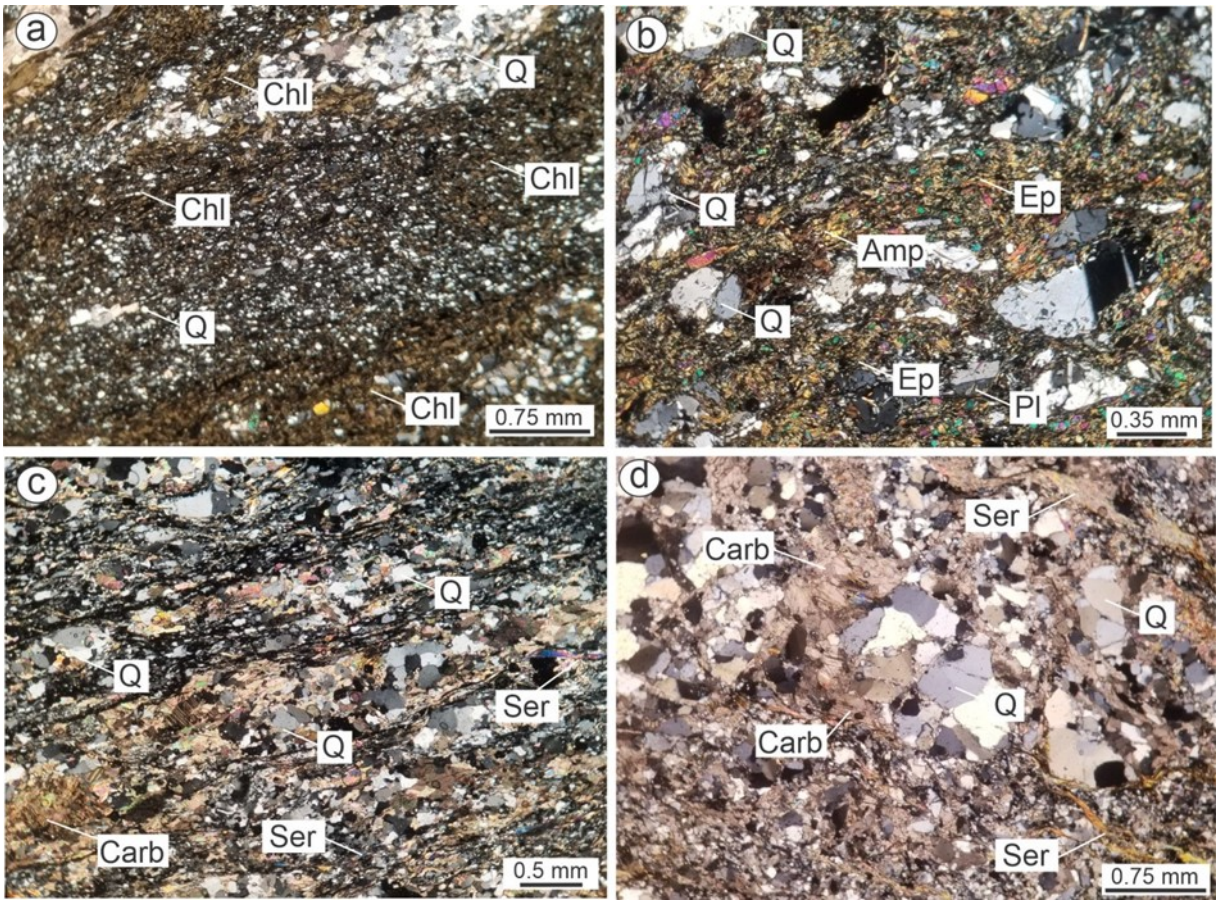

Fig. 5. Representative microphotographs of metamorphic rocks from the Emgentiin Bulag area. a) Quartz-chlorite schist (sample E6), b) Amphibole-chlorite schist (sample E7), c) Quartz-sericite schist (sample E2), d) Schistose sandstone (sample E4). Abbreviations: Q – quartz, Pl – plagioclase, Amp – amphibole, Ep – epidote, Chl – chlorite, Mus – muscovite, Ser – sericite, Carb – carbonate. All photomicrographs are under cross-polarized light.

quartz was recrystallized to a granular mosaic with serrated margins and together with plagioclase, ranges from 0.2 to 1.2 mm in size. The biotite is generally subidiomorphic and ranges from 0.1 to 1mm in length. Garnet is euhedral and about 1.8 - 2.0 mm in size (Fig. 4d). Quartz-muscovite schist (sample O46/1) contains quartz (Q, 55 -60%), muscovite (Mus, 40 – 45%). All the mica schists are fine- to medium grained, laminated, and well foliated. Its protolith was interpreted to be sedimentary rocks.

Emgentiin Bulag area

The Proterozoic sequences in the Emgentiin Bulag area are referred to upper member of Ereendavaa Formation with Mesoproterozoic (Blagonravov et al., 1968; Dorjnamjaa and Batireedui, 1991; Dorjnamjaa et al., 2012) or Neoproterozoic (Erdenechimeg et al., 2017) ages. The studied section is located in the north-western side of the Emgentiin Bulag spring (49^{o} 01’ 44.8’’; 112^{o} 06’ 22.0’’). The Ereendavaa Formation in this area mainly comprises a sequence of dark-green to light gray quartz-chlorite, amphibole-chlorite and quartz-sericite schist and schistose sandstone with total thickness of about 800 m (Fig. 2f).

Quartz-chlorite schist (sample E6) is composed quartz (Q, 30 - 35%) and chlorite (Chl, 55 – 60%) with minor amount of ilmenite (1 – 5%) and secondary calcite (Carb, 5 -10%) (Fig. 5a). The rock generally lepidogranoblastic in texture and strongly foliated, defined by aligned chlorite grains. The quartz is recrystallized to a granular mosaic with serrated

margins and ranges from 0.5 to 2 mm in size. Its protolith was interpreted to be volcanic rock.

Amphibole-chlorite schist (sample E7) is lepidogranoblastic in texture and comprises epidote (Ep, 10 – 15%), amphibole (Amp, 15 – 20%), chlorite (Chl, 20 -25%) and quartz (Q), plagioclase (Pl) aggregates (20 -30%) with minor amount of magnetite (3 – 5%). The schistosity is well defined by oriented green chlorite and amphibole alternating with felsic mineral aggregates (Fig. 5b). The typical mineral assemblage is Hbl+Chl+Ep+Q, and the rocks are considered to be mafic in origin.

Quartz-sericite schist (samples E2, E5) and **schistose sandstone** (samples E3, E4) are lepidoblastic in texture and generally have similar mineral assemblages. The rock consists of quartz (Q, 40 -50%), plagioclase (Pl, 1 – 2%) and composed of fine-grained quartz, sericitizated plagioclase cement (50 – 70%) with minor secondary biotite (Bt), calcite (Carb) and black colored opaque minerals and zircons (Fig. 5c and d) .The rock is strongly or slightly foliated, defined by aligned sericite flakes. Its protolith is interpreted to be sedimentary rocks.

ANALYTICAL METHODS

U-Pb zircon geochronology

Zircon crystals were obtained from crushed rock using a combination of heavy liquid and magnetic separation techniques at Institute of Geology of Mongolian Academy of Sciences. Individual crystals were handpicked, mounted on adhesive tape, then enclosed in epoxy resin and polished to about half of their thickness. Cathodoluminescence (CL) images were obtained using a JXA-8100 Electron Probe Microanalyzer with Mono CL4 Cathodoluminescence System (Gatan) for high-resolution imaging and spectroscopy in the Institute of Mineral Resource, Chinese Academy of Geological Sciences and Institute of Geochemistry of Chinese Academy of Sciences.

U–Pb dating of zircons from 6 representative samples gneiss, schist and schistose sandstone was performed for LA-ICP-MS dating at Institute of Geology, Chinese Academy of Geological Sciences and Guangzhou Institute of Geochemistry of Chinese Academy of Sciences. Sample mounts were placed in a sample cell designed by Laurin Technic Pty. Ltd, flushed with Ar and He. Laser ablation was accomplished using a pulsed Resonetic 193 nm ArF excimer laser, operated at a constant energy of 80 mJ, with a repetition rate of 8 Hz and a spot diameter of 31 μm. The ablated aerosol was carried to an Agilent 7500a ICP-MS by He gas via a Squid system to smooth signals. Data were acquired for 30 s with the laser off, and 40 s with the laser on, giving approximate 100 mass scans. Zircon TEMORA was used as the external standard to correct elemental fractionation, while zircon Plešovice (PL) was also used for quality control. Data reduction was performed off-line by ICPMSDataCal 7.2 (Liu et al., 2010). U-Pb ages of zircons were calculated using the U decay constants of $^{238}U=1.55125 \times 10^{-10}$ year^{-1}, $^{235}U=9.8454 \times 10^{-10}$ year^{-1} and the Isoplot 3 software (Ludwig, 2003).

Major and trace element analysis

Major element oxides (wt.%) of 11 samples were analyzed at the Acme Analytical Laboratories Ltd., Vancouver (Canada). Major element compositions and Sc, Ba, and Ni abundances were determined by inductively coupled plasma-atomic emission spectrometry (ICP-AES). The remainder of the trace elements and rare earth elements (REEs) was determined using inductively coupled plasma-mass spectrometry (ICP-MS) (for Acme codes 4A-4B and 1DX analytical procedures see http://acmelab.com). A total of 21 samples were analyzed for major element at SGS Mongolia (invested by Switzerland), using standard procedure (https://www.sgs.mn). Major element concentrations were analyzed by X-ray Fluorescence Spectrometry (XRF). For the major element analysis, glass beads were prepared by fusing mixtures of 0.7 g of powdered sample with 6.0 g of lithium tetraborate. Analytical uncertainties are generally better than 1%. Trace elements, including rare earth elements (REEs) of 21 samples were analyzed by a Perkin-Elmer Sciex ELAN 6000 ICP-MS, in the State Key Laboratory of Isotope Geochemistry, Guangzhou Institute of Geochemistry. Powdered

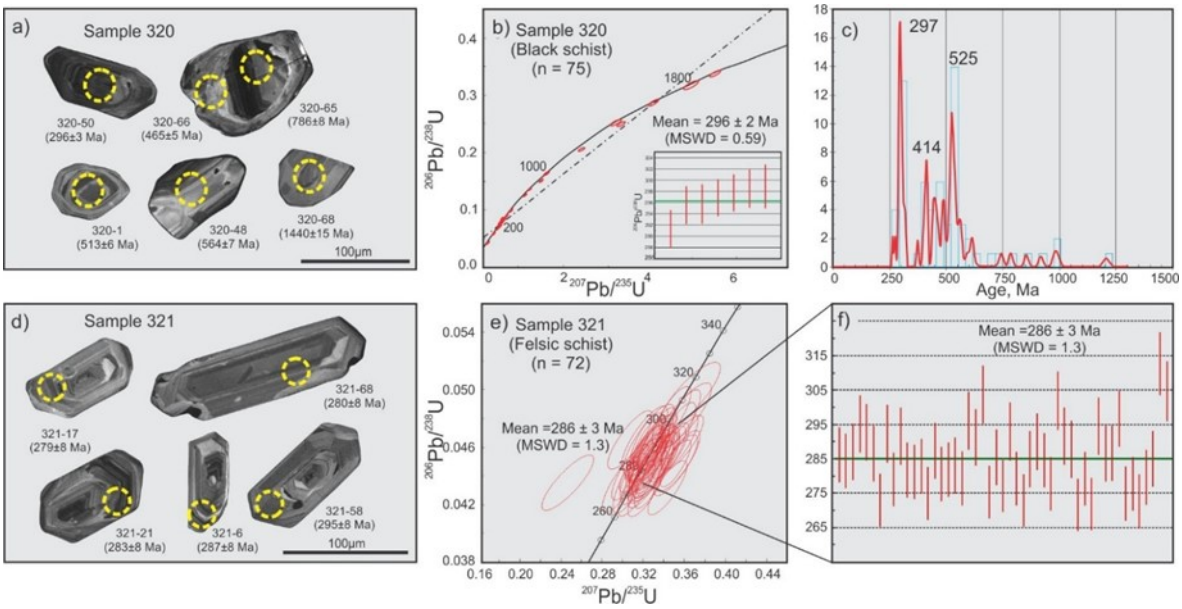

Fig. 6. CL images of typical zircons, zircon $^{207}Pb/^{235}U$ - $^{206}Pb/^{238}U$ concordia diagrams and age probability histograms of detrital zircons of Sample 320 (Black schist) and Sample 321 (Felsic schist) from Mogoitiin Gol area. The notation for each spot (a, d) consists of spot number and the $^{206}Pb/^{238}U$ age. Inserted small figures are weighted average ages of youngest zircon population of detrital zircons.

samples (50 mg) were digested with mixed HNO_3+HF acid in steel-bomb coated Teflon beakers for 2 days in order to assure complete dissolution of the refractory minerals. An internal standard solution containing the single element Rh was used to monitor signal drift. The USGS rock standards G-2, W-2, MRG-1 and AGV-1 and the Chinese national rock standards GSD-12, GSR-1, GSR-2 and GSR-3 were used to calibrate the elemental concentrations of the measured samples. Analytical precision was generally better than 5%. Sample preparation techniques and other details of procedures are described in the references (Yuan et al., 2010; Long et al., 2010).

RESULTS

Zircon U–Pb geochronology

Six representative samples of gneiss, schist and schistose sandstone considered typical for Khaychingol and Ereendavaa Formations were selected for LA-ICP-MS U-Pb zircon dating. They were collected along three sections, which are generally perpendicular strike of the strata and sample location are illustrated in Fig. 1d, e and f, and the analytical results are presented in Supplementary data, Table 1 and Figs. 6 and 7.

Mogoitiin Gol area

Sample 320 from the black schist was collected from the Mogoitiin gol area, in the southern part of Khaliun Mountain (location: 49°29'40.5''; 112°55'49.5''). Zircons from Sample 320 are colorless, with euhedral to subhedral shape. They range in length from ca. 50 to 130 μm, with length to width ratios of 1:1 to 2:1 (rare to 3:1). CL images reveal that most of grains are oscillatory zoned and few have a core-rim structure (Fig. 6a). Total of 75 analyses were made on 73 zircons (Fig. 6b). Th/U ratio of zircons is range from 0.15 to 2.20, except two low values of the rim. The detrital zircons have concordant ages ranging between 291 ± 4 Ma and 1892 ± 27 Ma with three age populations with conspicuous peaks at 525 Ma, 414 Ma and 297 Ma, respectively (Fig. 6c). Other concordant analyses define ages from 743 ± 9 Ma to 1892 ± 27 Ma without obvious peaks. Two analyses on the rim have concordant $^{206}Pb/^{238}U$ ages of 465 ± 5 and 522 ± 5 Ma. Their low Th/U ratios (0.004 and 0.03) may indicate that their ages record the time of high-grade metamorphism. The youngest coeval zircon grains between 291 ± 4 and 299 ± 3 Ma yield a weighted mean age of 296 ± 2 Ma (MSWD = 0.59, n = 7) which constrains the youngest depositional age of

protolith to be after 296±2 Ma (Fig. 6b).

Sample 321 from quartz-sericite schist was collected from the Mogoitiin Gol area, in the south of Khaliun Mountain (location: 49°29'45.9"; 112°55'46.6"). The zircon grains from the felsic schist sample mostly range from 60 to 160 μm in length with euhedral morphology (Fig. 6d). All the zircon grains display oscillatory growth zoning, consistent with an igneous origin (Koschek, 1993).

Total of 72 analyses were made on 65 zircons and 49 concordant analyses on zircon grains yield a weighted mean $^{206}Pb/^{238}U$ age of 286 ± 3 Ma (MSWD = 1.3, n = 49), which likely represents the crystallization age of the protolith (Table 1; Fig. 6e-f).

Khaychin Gol area

Sample O35 from biotite-plagioclase gneiss was collected from the Khaychin Gol area (location: 49°22'57.0''; 112°51'3.0''). Zircons from Sample O35 are colorless, with euhedral to subhedral shape. They range in length from ca. 50 to 150 μm, with length to width ratios of 1:1

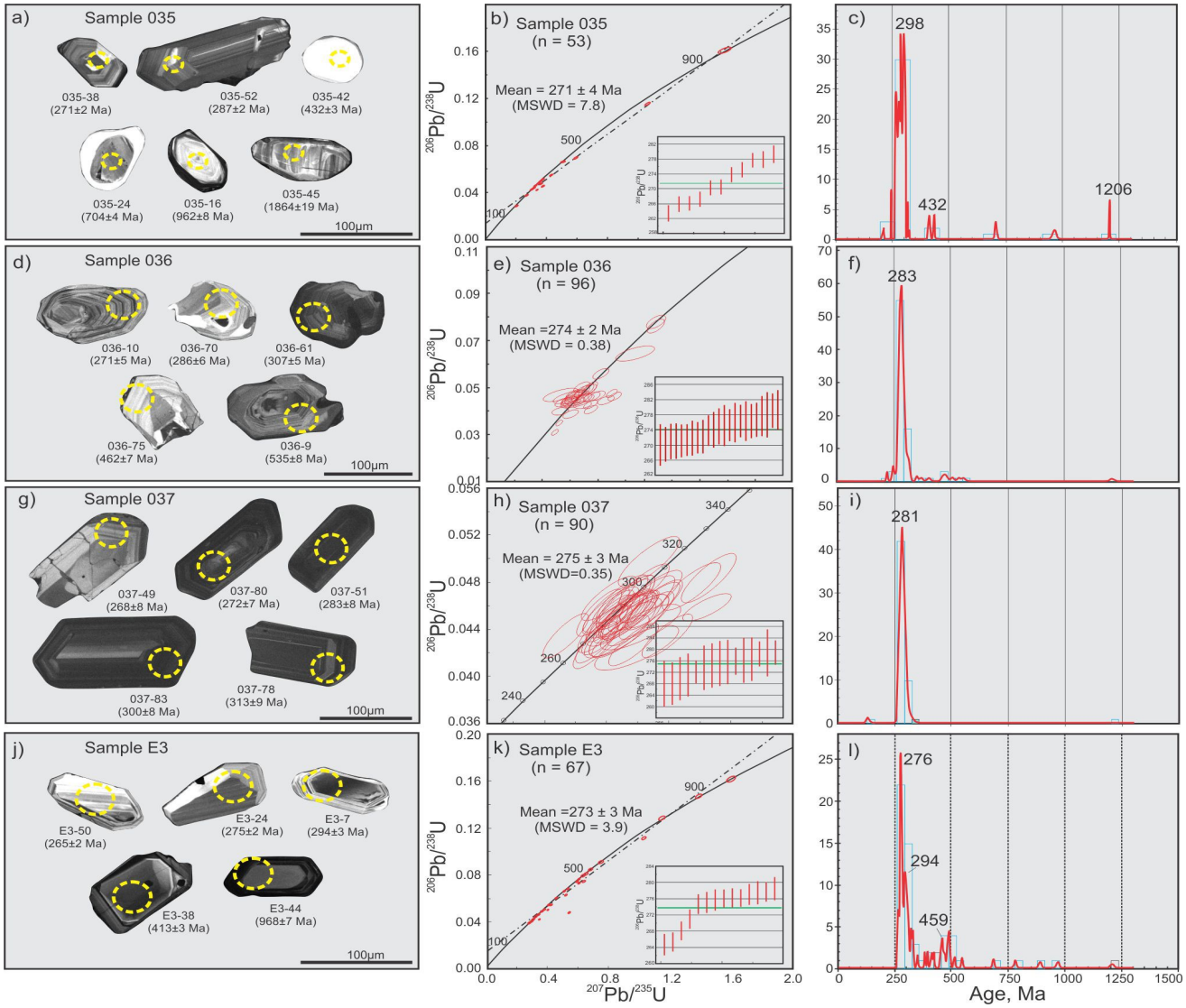

Fig. 7. CL images of typical zircons, zircon $^{207}Pb/^{235}U$ - $^{206}Pb/^{238}U$ concordia diagrams and age probability histograms of detrital zircons of Sample 035, 036, 037 (Biotite-plagioclase gneiss) from Khaychin Gol area and Sample E3 (Psammitic schist) from Emgentiin Bulag area. The notation for each spot (a, d, g, j) consists of spot number and the $^{206}Pb/^{238}U$ age. Inserted small figures are weighted average ages of youngest zircon population of each detrital zircon samples.

to 2:1 (rare to 3:1). CL images reveal that most of zircon grains are oscillatory zoned and few have a core-rim structure with very thin rims (Fig. 7a).

Totally, 53 zircons were analyzed. The Th/U ratios of zircons vary between 0.22 and 1.51. The high Th/U ratios of zircons (>0.1) and observed oscillatory growth zoning in CL images, suggest that most of the detrital zircons have a magmatic origin (Koschek, 1993). However, few zircons (see point 035-42 in the Fig. 7a) show white color in CL images, implying some loss of Pb. The detrital zircons have concordant ages range between 263 ± 2 Ma to 1864 ± 18 Ma with a single large population (72%) between 263 and 299 Ma, with prominent peak at 298 Ma. Other concordant analyses define ages from 300 ± 2 Ma to 1864 ± 18 Ma without obvious peaks. The youngest coeval zircon grains between 263 ± 2 and 279 ± 2 Ma yield a weighted mean age of 271 ± 4 Ma (MSWD = 7.8, n = 11) which constrains the youngest depositional age of protolith to be later than 271 ± 4 Ma (Fig. 7b-c).

Sample O36 from biotite-plagioclase gneiss was collected from the Khaychin Gol area (location: 49°23'04.7"; 112°50'57.0"). Zircons from Sample O36 are colorless, with euhedral to subhedral shape. They range in length from ca. 80 to 180 μm, with length to width ratios of 1:1 to 2:1 (rare to 3:1). CL images reveal that almost all of zircon grains are oscillatory zoned (Fig. 7d). Total of 96 analyses were made on 96 zircons. The detrital zircons have 78 concordant ages ranging between 265 ± 5 and 558 ± 8 Ma with a single large population between 258 and 299 Ma (79%) with a prominent peak at 283 Ma. Other concordant analyses (21%) define ages from 300 ± 2 Ma to 558 ± 8 Ma without obvious peaks. The youngest coeval zircon grains between 258 ± 6 and 279 ± 5 Ma yield a weighted mean age of 274 ± 2 Ma (MSWD = 0.78, n = 25) which constrains the youngest depositional age of protolith to be later than 274 ± 2 Ma (Fig. 7e-f).

Sample O37 from biotite-plagioclase gneiss was collected from the Khaychin Gol area (location: 49°23'03.0''; 112°50'56.9''). Zircons from Sample O37 are colorless, with euhedral to subhedral shape. They range in length from ca. 70 to 190 μm, with length to width ratios of 1:1 to 2:1. CL images reveal that all of zircon grains are oscillatory zoned (Fig. 7g). Total of 90 analyses were made on 90 zircons. The detrital zircons have 55 concordant ages ranging from 285 ± 7 to 325 ± 9 Ma with single large population with prominent peak at 281 Ma. The youngest coeval zircon grains between 268 ± 7 and 280 ± 4 Ma yield a weighted mean age of 275 ± 3 Ma (MSWD = 0.35, n = 15) which constrains the youngest depositional age of protolith to be later than 276±2 Ma (Fig. 7h-i).

Emgentiin Bulag area

Sample E3 from schistose sandstone was collected from the Emgentiin Bulag area (location: 49°01'49.5''; 112°06'34.1''). Zircons from Sample E3 are colorless, with euhedral to subhedral shape. They range in length from ca. 50 to 160 μm, with length to width ratios of 2:1 to 3:1. CL images reveal that all of zircon grains are oscillatory zoned (Fig. 7j). Total of 67 analyses were made on 67 zircons. The Th/U ratios of zircons vary between 0.11 and 2.2. The high Th/U ratios of zircons (>0.1) and observed oscillatory growth zoning in CL images, suggest that the most detrital zircons were derived from a magmatic provenance (Koschek, 1993). The detrital zircons have 58 concordant ages ranging from 265 ± 3 to 968 ± 7 Ma. Most of them show concordance more than 90% and yield ages mainly clustering at ca. 265 - 299 Ma and ca. 448 - 500 Ma, with the prominent age peak at ca. 276 Ma and minor peaks at ca. 294 Ma and 459 Ma, respectively. The youngest coeval zircon grains between 265 ± 3 and 279 ± 4 Ma yield a weighted mean age of 273 ± 3 Ma (MSWD = 3.9, n=10) which constrains the youngest depositional age of protolith to be later than 273 ± 3 Ma (Fig. 7k-l).

Whole-rock geochemistry

The results of major and trace element analysis of the 32 schist and gneiss samples from the Mogoitiin Gol, Khaychin Gol and Emgentiin Bulag areas are listed in Supplementary data, Table 2 and 3.

Schist sequence of the Mogoitiin Gol area

According to the field investigation and thin

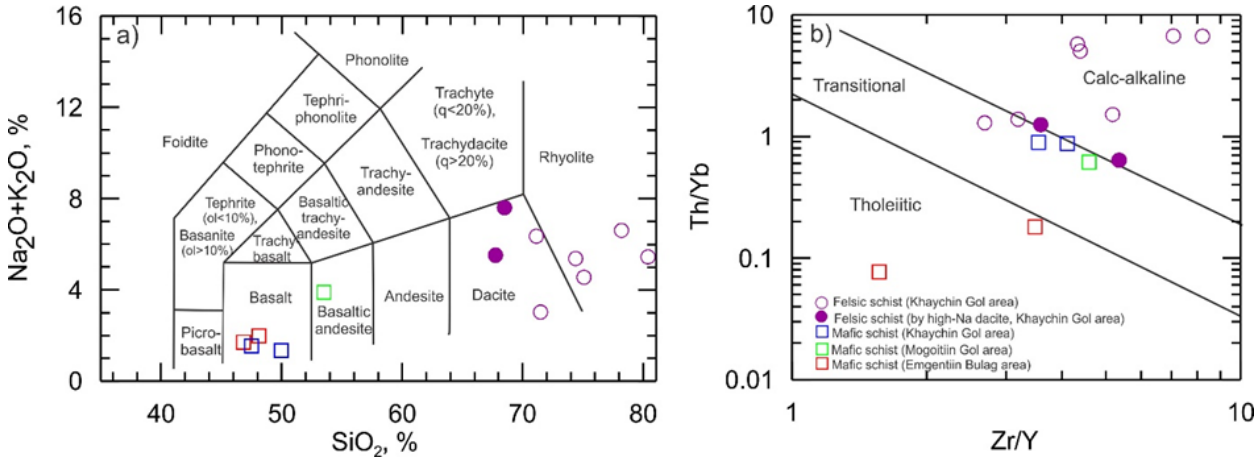

Fig. 8. Classification diagrams of the mafic and felsic schists from the Mogoittin Gol, Khaychin Gol and Emgentiin Bulag areas. a) SiO2 vs. (Na_2O+K_2O) classification diagram (Le Maitre, 1989); b) Th/Yb vs Zr/Y discrimination diagram (Ross and Bédard, 2009)

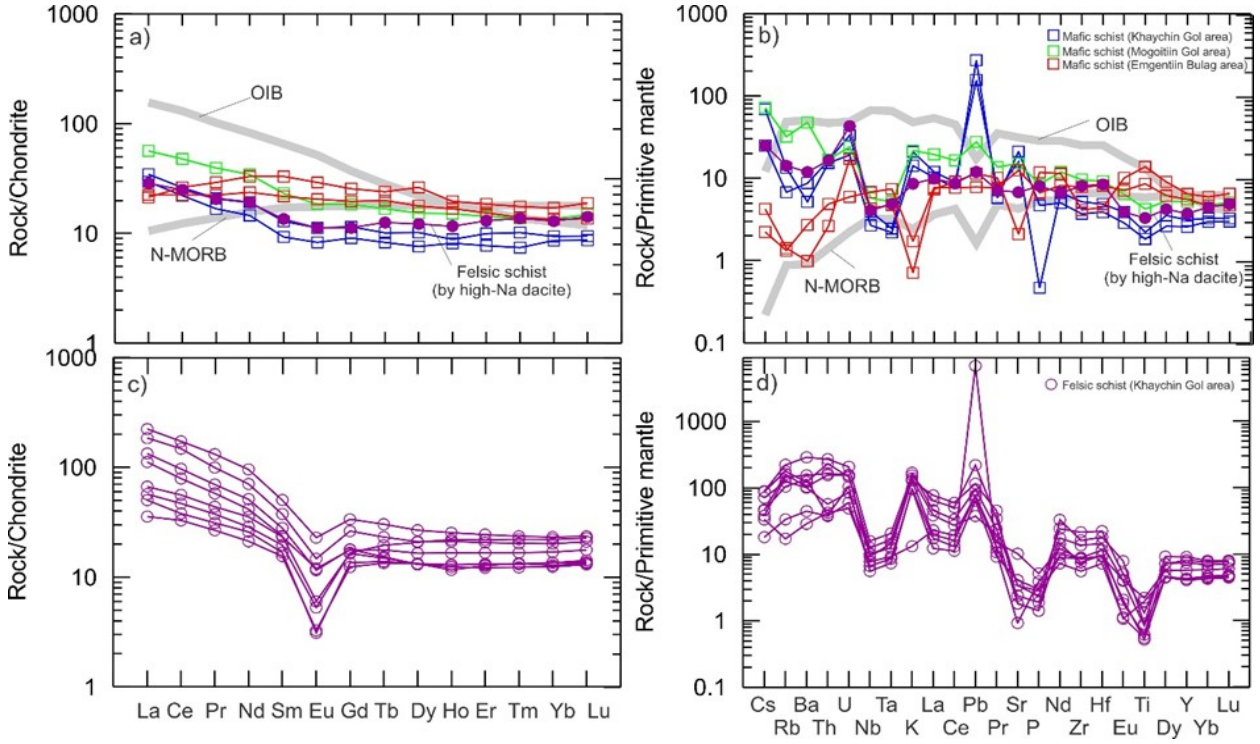

Fig. 9. Chrondrite-normalized REE patterns and primitive mantle-normalized trace element spider diagrams for studied mafic and felsic schists. Chondrite- and primitive mantle-normalization values are from Sun and McDonough (1989). OIB and N-MORB data from Sun and McDonough (1989) are plotted for comparison, respectively. OIB, Oceanic island basalt; N-MORB, Normal mid-ocean ridge basalt.

section observation, felsic schists (quartz-sericite and chlorite-quartz schists) with minor intercalation of mafic (hornblende schist) and black schists are the most common varieties of metamorphic rocks within the studied section in the Mogoitiin Gol area.

Mafic schist

Major elements. Mafic schist has low SiO_2 (53.5 wt.%) and alkali (K_2O + Na_2O = 3.89 - wt.%) contents. The rock also shows high Al_2O_3 (17.7 wt.%) and $Fe_2O_3^T$ (11.4 wt.%), and intermediate MgO (4.98 wt.%) contents and

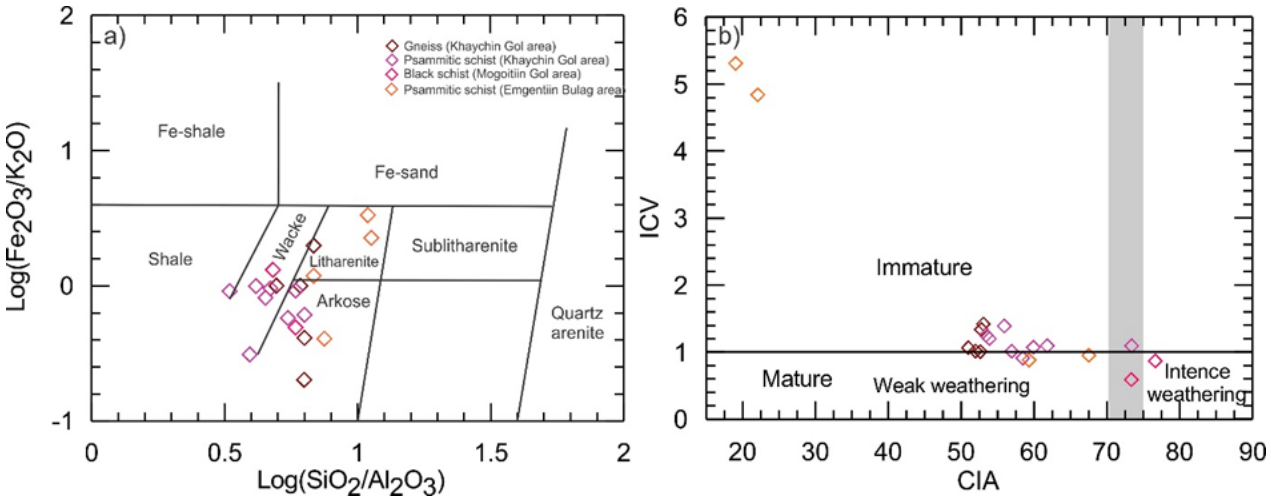

Fig. 10. Classification diagrams of black schist, gneiss and psammitic schist from the Mogoittin Gol, Khaychin Gol and Emgentiin Bulag areas. a) Log (SiO_2/Al_2O_3) vs. log(Fe_2O_3/K_2O) classification diagram (Herron, 1988); b) CIA–ICV diagram (after Nesbitt and Young, 1984).

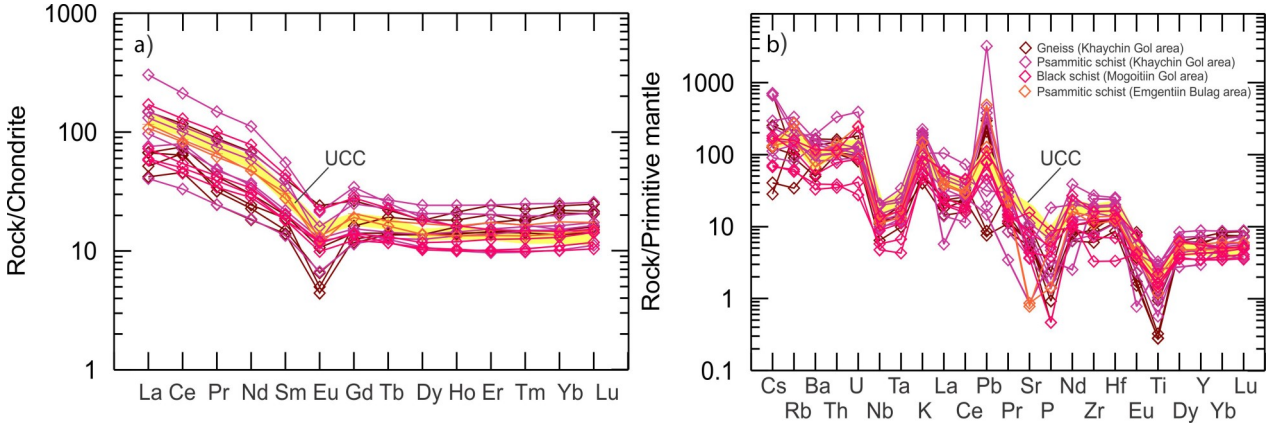

Fig. 11. Chrondrite-normalized REE patterns and primitive mantle-normalized trace element spider diagrams for of black schist, gneiss and psammitic schists from the Mogoittin Gol, Khaychin Gol and Emgentiin Bulag areas. Chondrite- and primitive mantle-normalization values are from Sun and McDonough (1989). UCC data from Taylor and McLennan (1985) are plotted for comparison, respectively. UCC, Upper continental crust.

Mg# value (50) (Table 2). On a total alkali versus silica (TAS) diagram, the rock is plotted into the basaltic andesite field (Fig. 8a). Geochemically, such rock belongs to the transitional tholeiitic series (Fig. 8b). The A/CNK and A/NK ratios are 0.91 and 2.93, respectively, corresponding to a metaluminous type (Table 2).

Trace elements. The mafic schist is characterized by enrichment of LREE relative to HREE (La_n/Yb_n = 4.13, La_n/Sm_n = 2.44) (Fig. 9a). On primitive mantle normalized plots, the rock exhibits slight enrichment of Cs, Ba, U, K and Pb, and depletion of Nb, Ta, Sr and Ti relative to adjacent elements (Fig. 9b).

Felsic schist

Major elements. On a total alkali versus silica (TAS) diagram, the samples from felsic schist are plotted in rhyolite and dacite fields (Fig. 8a). The rhyolite and dacite have high SiO_2 (67.8 – 80.4 wt.%), Al_2O_3 (12.2 - 17.5 wt.%) contents and alkali (K_2O + Na_2O = 3.02 - 7.60 wt.%) values. The rhyolites are characterized by low Na_2O (0.06 – 1.70 wt.%) and high K_2O (2.96 – 5.08 wt.%) contents, while the dacites have high Na_2O and low K_2O contents ranging between 5.25 – 7.20 wt.% and 0.26 – 0.40 wt.%, respectively. Both of them have low $Fe_2O_3^T$ (1.09 - 4.92 wt.%), as well as relatively low MgO (0.32 - 2.64 wt.%) and CaO (0.04 – 0.84 wt.%) contents, except sample 321 with

intermediate MgO (6.22 wt.%) and sample 324/1 with intermediate $Fe_2O_3^T$ (7.54 wt.%) (Table 2).

In a plot of Th/Yb versus Zr/Y variation diagram, the rhyolites and dacites fall in the calc -alkaline and transitional tholeiitic series (Fig. 8b). The A/NK (molar $Al_2O_3/(Na_2O + K_2O)$) and A/CNK (molar $Al_2O_3/(CaO + Na_2O + K_2O)$) values of these rocks range from 1.29 to 4.14 and from 1.14 to 3.95, respectively, indicating that these rocks are all peraluminous (Table 2).

Trace elements. The rhyolites are all enriched in LREE (La_n/Yb_n = 2.22 - 10.76) and display relatively flat HREE patterns with obvious negative Eu anomalies (Eu/Eu* = 0.21 - 0.59) (Table 2; Fig. 9c), while the dacites have almost flat chondrite-normalized REE patterns (Eu/Eu* = 0.91 for sample 324/1) parallel to those of the mafic schist (Fig. 8a). A primitive-mantle normalized trace element spider diagram indicates that these rocks are enriched in LILEs (e.g., Cs, Rb, Ba and K) and depleted in HFSEs (e.g. Nb, Ta and Ti) (Fig. 8d).

Black schist

Major elements. The black schist has high SiO_2 (72.4 – 78.9 wt.%) and Al_2O_3 (13.5 – 15.1 wt.%) contents with $Fe_2O_3^T$ values varying from 2.18 wt.% to 5.80 wt.% (Table 3). On a log ($Fe_2O_3^T/K_2O$) versus log (SiO_2/Al_2O_3) (Herron, 1988) diagram, the samples from black schist are plotted in the wacke and arkose fields (Fig. 10a).

Trace elements. The black schist is characterized by LREE enrichment (La_n/Yb_n = 6.62 – 7.73, La_n/Sm_n = 3.80 – 3.88) and moderate negative Eu anomalies (Eu/Eu* = 0.45 – 0.48) (Table 3; Fig. 11a). The schists are enriched in Pb and depleted in Sr and P with respect to UCC as shown by primitive mantle-normalized multi-element distribution patterns (Fig. 11b).

In addition, the black schist has high concentrations of U (5.2 ppm), As (563 ppm) and Sb (5 ppm) compared with UCC (U - 2.8 ppm, As - 1.5 ppm, Sb - 0.2 ppm).

Gneiss and schist sequence of Khaychin Gol area

The metamorphic rocks in this area mainly comprise a sequence of garnet and tourmaline bearing gneiss (biotite-plagioclase gneiss) and psammitic schist (mica schists) with sedimentary protolith and contain minor mafic (hornblende schist) schist with igneous protolith.

Mafic schist

Major elements. Mafic schist from the Khaychin Gol area have whole-rock SiO_2 contents of 47.5 - 49.9 wt.%, and relatively low alkali contents ($K_2O + Na_2O$ = 1.34 - 1.54 wt.%). Consequently, on the total alkali versus silica (TAS) diagram, the mafic schists are plotted in basalt field (Fig. 8a), and they show characteristics of transitional toleiitic basalt (Fig. 8b). The rocks also show high Al_2O_3 (12.7 - 13.5 wt.%), $Fe_2O_3^T$ (9.72 – 12.5 wt.%), CaO (14.1 – 14.9 wt.%), and MgO (9.78 – 10.8 wt.%) contents as well as high Mg# values (65 - 70) (Table 2). The A/NK and A/CNK values of these rocks range from 5.86 to 6.87 and from 0.49 to 0.79 and respectively, indicating that these rocks are all metaluminous (Table 2).

Trace elements. The mafic schists are characterized by enrichment of LREE relative to HREE (La_n/Yb_n = 3.44 – 3.68, La_n/Sm_n = 2.69 – 3.18) without significant Eu anomalies (Fig. 9a). On primitive mantle normalized plots, these rocks exhibit enrichment of Cs, U, Pb and Sr and depletion of Rb, Ba, Nb, Ta, Ti and P relative to adjacent elements (Fig. 9b).

Garnet bearing biotite-plagioclase gneiss

Major elements. The gneisses from the Khaychin Gol area have high SiO_2 (70.7 – 78.2 wt.%) and Al_2O_3 (11.3 – 14.2 wt.%) contents with low $Fe_2O_3^T$ (1.13 - 4.17 wt.%) and variable Na_2O and K_2O values ranging from 2.51 to 5.48 and from 1.20 to 5.59 wt.%, respectively (Table 3). On a log ($Fe_2O_3^T/K_2O$) versus log (SiO_2/Al_2O_3) (Herron, 1988) diagram, the samples from gneisses are plotted mainly in the arkose field (Fig. 10a).

Trace elements. The gneiss is characterized by enrichment of LREE (La_n/Yb_n = 2.37 – 7.09, La_n/Sm_n = 3.00 – 3.67) and moderate negative Eu anomalies (Eu/Eu* = 0.29 – 0.74) (Table 3; Fig. 11a). Primitive mantle-normalized multi-element distribution diagrams show enrichment of Rb, Th, U, K, and Pb, and depletion of Nb,

Ta, P and Ti, sharing common features of with that of UCC (Fig. 11b).

Psammitic schist

Major elements. The mica schists from the Khaychin Gol area have high SiO_2 (67.8 – 77.9 wt.%) and Al_2O_3 (12.1 – 19.0 wt.%) contents with low $Fe_2O_3^T$ (1.79 - 6.16 wt.%) and variable Na_2O and K_2O values ranging from 0.18 to 3.22 and from 2.01 to 6.74 wt.%, respectively (Table 3). On a log ($Fe_2O_3^T/K_2O$) versus log (SiO_2/Al_2O_3) (Herron, 1988) diagram, the samples from schists are plotted mainly in the arkose and wacke fields (Fig. 10a).

Trace elements. Chondrite-normalized REE distribution patterns show LREE enrichment (La_n/Yb_n = 1.01 – 3.01, La_n/Sm_n = 3.01 – 5.63) and moderate negative Eu anomalies (Eu/Eu* = 0.35 – 0.86) (Table 3; Fig. 11a). Primitive mantle-normalized multi-element distribution diagrams show enrichment of Th, U, K and Pb, depletion of Nb, Ta, P and Ti, (same as gneiss) sharing common features of UCC (Fig. 11b).

Schist sequence of the Emgentiin Bulag area

The metamorphic rocks in this area mainly comprise a sequence of psammitic schist (quartz -sericite schist and schistose sandstone) with sedimentary protolith and contain lenses of mafic (quartz-chlorite and amphibole-chlorite schist) schist with igneous protolith.

Mafic schist

Major elements. Mafic schists from the Emgentiin Bulag area have low whole-rock SiO_2 contents of 46.8 - 48.1 wt.%, and low alkali contents (K_2O + Na_2O = 1.70 - 1.98 wt.%). Consequently, on the total alkali versus silica (TAS) diagram, the mafic schists are plotted in the basalt field (Fig. 8a), and they show characteristics of toleiitic basalt (Fig. 8b). The rocks also show high Al_2O_3 (14.9 - 15.6 wt.%), $Fe_2O_3^T$ (14.7 – 20.3 wt.%), CaO (2.66 – 10.7 wt.%) and MgO (7.53 – 9.66 wt.%) contents and as well as high Mg# values (53 - 54) (Table 2). The A/NK and A/CNK values of these rocks range from 4.63 to 5.61 and from 0.66 to 2.04,

respectively, indicating that these rocks are metaluminous to peraluminous (Table 2).

Trace elements. In chondrite-normalized REE distribution patterns, the mafic schist has slight LREE enrichment relative to HREE (La_n/Yb_n = 1.24 – 1.68, La_n/Sm_n = 0.65 – 1.03) without Eu anomalies (Eu/Eu* = 0.99 – 1.00) (Table 2; Fig. 9a). On primitive mantle normalized plots, these rocks exhibit enrichment of Cs, U, and Ti and depletion of Rb, Ba, Sr and K relative to adjacent elements (Fig. 9b).

Psammitic schist

Major elements. These rocks have high SiO_2 (72.3 – 82.0 wt.%) and Al_2O_3 (6.40 – 11.5 wt.%) contents with low $Fe_2O_3^T$ (0.96 - 4.67 wt.%) and variable Na_2O and K_2O values ranging from 0.01 to 2.84 and from 1.40 to 2.90 wt.%, respectively (Table 3). On a log ($Fe_2O_3^T/K_2O$) versus log (SiO_2/Al_2O_3) (Herron, 1988) diagram, the samples from schists and metasandstones are plotted mainly in the arkose and litharenite fields (Fig. 10a).

Trace elements. Chondrite-normalized REE distribution patterns show LREE enrichment (La_n/Yb_n = 4.43 – 11.7, La_n/Sm_n = 3.20 – 3.90) and moderate negative Eu anomalies (Eu/Eu* = 0.63 – 0.75) (Table 3; Fig. 11a). Primitive mantle-normalized multi-element distribution diagrams show enrichment of Th, U, K and Pb, depletion of Nb, Ta, P and Ti, same as gneiss and schists from Khaychin Gol and Mogoittin Bulag areas, sharing common features of UCC (Fig. 11b).

DISCUSSION

Formation/Deposition time of studied metamorphic rocks

Zircon U-Pb data for the felsic schist from the Mogoitiin Gol area yield a crystallization age of 286 ± 3 Ma (Table 1; Fig. 6e). CL images of zircons reveal euhedral shapes and typical oscillatory growth zoning, consistent with an igneous origin (Koschek, 1993). In addition, the youngest age population of the black schist from this area is 296 ± 2 Ma and these zircons have oscillatory growth zoning and a relatively high Th/U ratio of 0.15 - 2.20, indicating a magmatic origin (Table 1, Fig. 6a-c). Therefore, we regard 296 Ma as the best estimate for the maximum deposition age of the black schist and 285 Ma as the protolith age of the felsic schist.

A total of 224 analyzes with discordance less

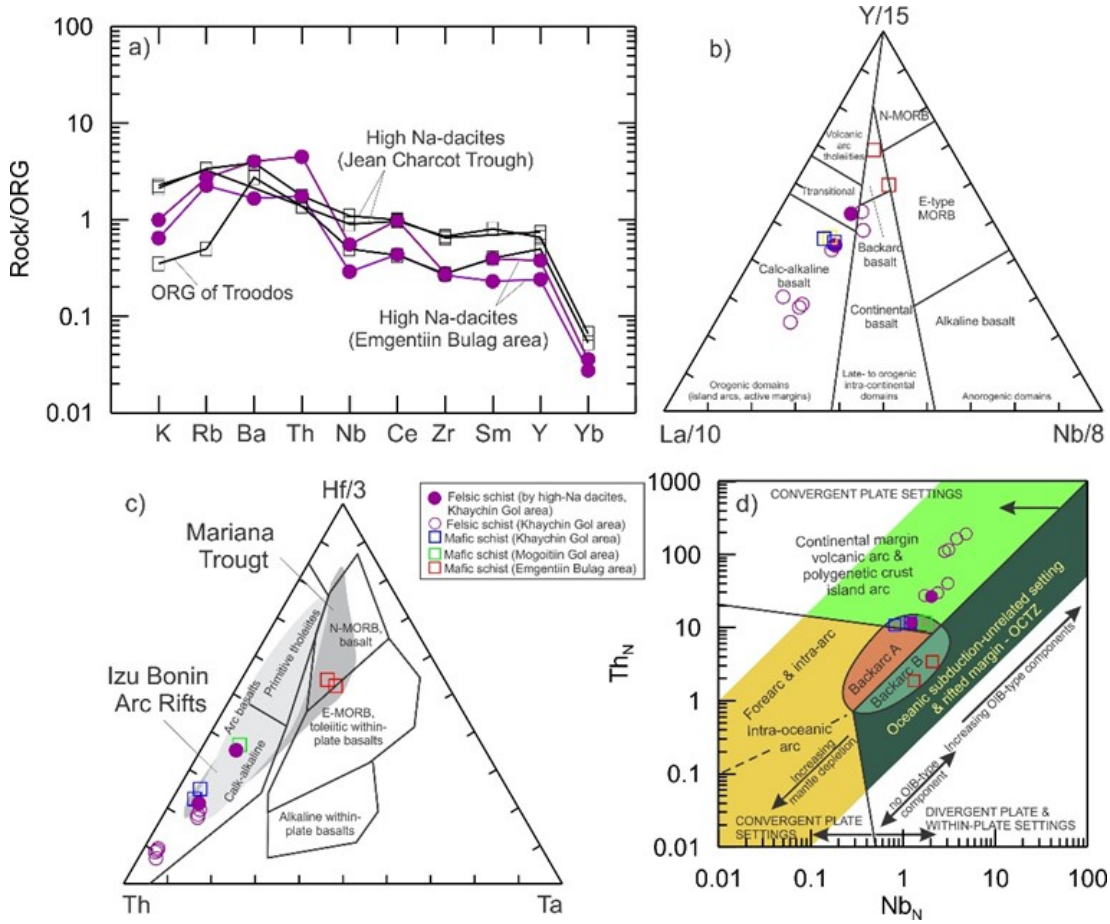

Fig. 12. a) Comparison of incompatible element patterns of the High-Na dacites from the Mogoitiin Gol area, Ereendavaa terrane and Troodos ocean ridge granite (ORG) and Jean Charcoat Trough, Southwest Pacific (Nakada et a., 1994). Normalizing values of ORG is from Pearce et al (1984); b) Y/15 – La/10 – Nb/8 (Cabanis and Lecolle, 1989) and c) Hf/3 – Th – Ta (Wood 1980) tectonic discrimination diagrams; d) Tectonic interpretation diagram of ophiolitic basaltic types based on Th_N -Nb_N systematics (Saccani, 2015) for the mafic and felsic schists. N-MORB, normal mid-ocean ridge basalt; E-MORB, enriched mid-ocean ridge basalt.

than 10% from four samples of gneiss and psammitic schists from the Khaychin Gol and Emgentiin Bulag areas yield apparent ages from 1809 to 263 Ma (Table 1). Zircons from these samples exhibit oscillatory growth zoning and high Th/U ratios (0.22 – 1.51), indicative of a magmatic origin, suggesting that the obtained U -Pb ages represent the timing of crystallization of the zircons (Koschek, 1993). Therefore, the youngest age populations of these zircon samples, namely 271 ± 4 Ma for sample 035, 274 ± 2 Ma for sample 036, 276 ± 2 Ma for sample 037 and 273 ± 3 Ma for sample E3, imply that their maximum deposition ages are ~276 - 271 Ma (Table 1; Fig. 7). A granitic intrusion of Middle Permian Ulz complex (270 – 230 Ma, Erdenechimeg et al., 2017) which are intruded into the Ereendavaa Formation can be represent an upper age limit of gneisses and psammitic schists.

Taken together, LA–ICP–MS zircon U–Pb dating results indicate that the protolith of the studied metamorphic rocks from the north-eastern part of the Ereendavaa terrane were formed in two stages: 1) ~ 296 - 285 Ma, for the formation of protolith of felsic and black schists, which were previously believed to be Mesoproterozoic or Neoproterozoic in age; 2) ~276 - 271 Ma for the deposition of protolith of gneiss and psammitic schists, which were believed before to be Paleoproterozoic and Mesoproterozoic in age. For the mafic schists,

we assume that these rocks do not belong to the Middle Permian strata and can be represent an Early Permian bimodal association together with felsic schists. Presence of Early Permian bimodal association is supported by the new ages recently obtained from the magmatic rocks in the north-eastern part of the Ereendavaa terrane. For example, mylonitic granites (sample MO93 and MO98), augen gneiss (sample MO99) and amphibolite (sample MO89) which are located in the north-east of the Mogoitiin Gol area have protolith ages of 296 ± 5 Ma, 289 ± 5 Ma, 295 ± 5 Ma and 295 ± 3 Ma, respectively (Miao et a., 2017). Early Permian magmatic activity is also supported by the occurrence of 283 ± 5 Ma and 282 ± 7 Ma orthogneises from the central part of the Ereendavaa Range (Dauodene et al., 2013).

Considering a close spatial relationship of the Ereendavaa terrane with the Mongol-Okhotsk Belt in the north-west, we propose that the Early Permian bimodal magmatism and deposition of the protolith of the Early Permian black schist and Middle Permian gneiss and psammitic schist, are likely related to the evolution of the Mongol-Okhotsk Ocean.

Nature and tectonic setting of the Early to Middle Permian metamorphic rocks

The schist and gneiss samples from the north-eastern part of the Ereendavaa terrane have low LOI (mostly <3.5 wt.%) values, except few samples which show high LOI values ranging from 3.92 to 11.4 (Table 2). In the chondrite-normalized REE and primitive mantle-normalized trace element spider diagrams, the studied metamorphic rocks exhibit coherent pattern for REE and HFSE, indicating that these elements are relatively immobile during the metamorphism. Besides, LILEs also exhibit similar patterns (Figs. 9 and 11), suggesting that the LILEs are not considerably affected by the metamorphism. In addition, the $(Th/La)_{PM}$ and $(Nb/La)_{PM}$ ratios of these rocks mostly remain constant and do not show significant correlations with the loss on ignition, also supporting the low mobility of HFSE and REE (except Eu). Thus, our discussion on the affinity and tectonic setting of the Early Permian bimodal magma association and source-area weathering, provenance characteristics and tectonic setting of the Early and Middle Permian gneiss and schist are based mainly on the immobile HFSE and REE and some LILE.

Affinity and tectonic setting of the Early Permian mafic and felsic schists

The Early Permian mafic schists from the Mogoitiin Gol and Khaychin Gol areas have lower TiO_2 (0.40 – 0.92 wt.%), K_2O (0.45 – 0.63 wt.%), and MgO (4.98 – 10.8 wt.%) contents and slightly higher Al_2O_3 (13.5 – 17.7 wt.%) and Fe2O3 (9.79 – 12.5 wt.%) contents (Table 2) than the average MORB composition (Gale et al., 2013). In contrast, their SiO_2 (mean 49.2 wt.%) and CaO (mean 12.1 wt.%) contents are within the MORB range. The lower MgO and TiO_2 coupled with higher Al_2O_3 contents of these schists are similar with the main characteristics of back-arc basin basalts (BABB) (Langmuir et al., 2006; Gale et al., 2013). Furthermore, the mafic schists are characterized by slight enrichment of LREE relative to HREE (La_n/Yb_n = 4.13, La_n/Sm_n = 2.44 (Fig. 9a) and on primitive mantle normalized plots, these rocks exhibit enrichment of fluid-mobile elements of Cs, Rb, Ba, U, Pb and Sr, and depletion of Nb, Ta and Ti (Fig. 9b), almost identical with BABB (Gale et al., 2013). It appears therefore that Cs is delivered preferentially by the fluid component affecting BABB and that Ba and Rb have similar fluid mobility (Gale et al., 2013). In addition, high Ba/Th (mean = 101) and low Nb/U (mean = 5.61), Ce/Pb (mean = 2.17), Th/U (mean = 2.69), Ba/Cs (mean = 78.9) and Rb/Cs (mean = 6.03) ratios of mafic schists support this point, because, the distinctly low concentrations of moderately incompatible trace elements are one of the main characteristics of the trace element composition of BABB (Gale et al., 2013). In contrast, the mafic schists from Emgentiin Bulag area characterized by higher TiO_2 (1.85 – 2.98 wt.%), Fe_2O_3 (14.7 – 20.3 wt.%) and lower CaO (2.66 – 10.7 wt.%) and K_2O (0.02 – 0.05 wt.%) contents than average MORB composition (Gale et al., 2013). Overall, their REE and trace element distribution patterns are similar to N-MORB basalts, except slight enrichment of Ti and strong depletion of K (Fig. 9a, b).

As mentioned above, the Early Permian felsic schists have rhyolitic and dacitic compositions. The high SiO_2 (75.1 – 80.4 wt.%) and high-K calc-alkaline geochemical characteristics of the rhyolites together with LILE and LREE enrichment and HFSE depletion in primitive mantle-normalized spider diagrams (Fig. 8a and b, Fig. 9c and d) imply that the primary magma was derived by partial melting of crustal materials. In addition, obvious negative Eu anomalies (Eu/Eu* = 0.21 - 0.59) suggest that plagioclase was a residual phase in the magma source. However, rhyolites are depleted in Na_2O (1.11 – 1.70 wt.%, mean 1.11 wt.%), while dacites are (67.8 – 68.5 wt.% SiO_2) enriched in Na_2O (5.25 – 7.20 wt.%, mean 6.22 wt.%). Also, the dacites are characterized by flat chondrite-normalized REE pattern with slight enrichment of LREE, parallel to those of mafic schists from the Mogoitiin Gol and Khaychin Gol areas (Fig. 9a). Moreover, the dacites show enrichment of fluid-mobile elements of Cs, Rb, Ba, U, Pb and Sr, and depletion of Nb, Ta and Ti and have similar pattern to those of mafic schist (Fig. 9b). Almost identical incompatible element distribution patterns of the high Na-dacites (felsic schist) and low-K basalts (mafic schist) suggest that a petrogenetic relationship link between these magma types.

High-Na dacites compositionally resemble trondhjemite or oceanic plagiogranite (Barker, 1979). Incompatible element patterns of high-Na dacites form the Mogoitiin Gol area normalized to Ocean ridge granite (ORG) of Pearce et al (1984) are given in Fig. 12a. Except slight enrichment in LILE (K, Rb, Ba and Th), the high Na-dacites are close to the Troodos Ocean Ridge plagiogranite and comparable to the High-Na dacites from the Jean Charcoat Trough (Vanuatu), Southwest Pacific (Nakada et a., 1994).

As the ORG magma type is interpreted to have evolved via simple fractional crystallization of N-MORB (Pearce et al., 1984), our data suggest that the high-Na dacites from the Mogoitiin Gol area could be generated by extensive fractionation of a slightly LILE-enriched BABB or transitional-MORB.

In addition, the observed SiO_2 bimodality with a gap between 67.8 and 53.5 wt.% for the felsic and mafic schists also might be explained by partial melting of basaltic crustal materials. However, strong trace element similarities between mafic schist (basalt) and high-Na dacites indicative that the fractionation of low-K basalts had played a main role (Crawford et al., 1988). The Na_2O contents of the felsic (rhyolite) and mafic (basalt) schists are not high compared with dacites (Table 2). This implies that high-Na characteristics of dacites must be acquired during the differentiation process of the basaltic magmas and dacites can be derived from the low-K basalts via crystal fractionation (Nakada et al., 1994).

Thus, the geochemistry data of felsic and mafic schists from the Mogoitiin Gol area indicative that an Early Permian bimodal association may formed in a back-arc basin environment. This conclusion is also supported by the various immobile trace elements discriminant diagrams for tectonic setting. For example, the mafic schists from the Mogoitiin Gol, Khaychin Gol and Emgentiin Bulag areas together with high-Na dacites are plotted in the calk-alkaline and BABB, N-MORB basalt fields in the Y/15 – La/10 – Nb/8 (Cabanis and Lecolle, 1989) and Hf/3-Th-Ta (Wood, 1980) ternary diagrams (Fig. 12b and c), which are compatible with the fields for typical BABB ((e.g. Mariana Trough (Pearce et al., 2005)) and basalts from extensional rift basins behind the Izu-Bonin arc (Hochstaedter et al., 2001).

Backarc basin basalts (BABB) may form in both oceanic and continental backarc basins as a result of seafloor spreading in ensimatic and ensialic settings, respectively (Dilek and Furnes, 2011). Therefore, we have used Th_N versus Nb_N systematics of Sassani (2015) to infer the nature of the Early Permian mafic schists from the north-eastern part of the Ereendavaa terrane. As shown in the Fig. 12d, mafic schists and high-Na dacites from the Mogoitiin Gol area and the mafic schists from the Khaychin Gol areas plot in the 'Backarc-A' field, while mafic schists from the Emgentiin Bulag area plot in the 'Backarc-B field'. As suggested by Sassani (2015), 'Backarc A' indicates backarc basin basalts characterized by input of subduction or crustal components (e.g., immature intra-oceanic or ensialic backarcs), whereas 'Backarc B'

indicates BABBs showing no input of subduction or crustal components (e.g., mature intra-oceanic backarcs).

Thus, we can propose that, the back-arc bimodal magmatism in the north-eastern part of the Ereendavaa terrane, probably happened in response to upwelling of asthenospheric mantle and partial melting of the overlying mantle enriched by crustal materials, as BABBs commonly derived from partial melting of ascending N-MORB source-like asthenosphere, as a consequence of the back-arc rifting (Taylor and Martinez, 2003; Pearce and Stern, 2006).

Source-area weathering, provenance and tectonic setting of the Early Permian black schist and Middle Permian gneiss and psammitic schists

The chemical index of alteration (CIA) and index of compositional variation (ICV) can be used for quantitative evaluation of weathering degree of rocks (Nesbitt and Young, 1982; Cox et al., 1995). CIA and ICV for the Early Permian black schists from the Mogoitiin Gol area have an average value of 75 and 0.73, respectively, indicating intense weathering at the source area. In contrast, CIA and ICV values of the Middle Permian gneiss and psammitic schist from the Khaychin Gol and Emgentiin Bulag areas ranging between 51 and 68 and between 0.88 and 1.42, respectively indicating low degrees of weathering at the source (Fig. 10b, Table 3). Exceptions are two carbonate schist samples showing extremely low CIA (19 - 22) and high ICV (4.84 – 5.31) values (Fig. 10b, Table 3).

According to the Al_2O_3 – (CaO* + Na_2O) – K_2O (A-CN-K) diagram, Middle Permian gneiss and psammitic schist mainly fall in the granodiorite -

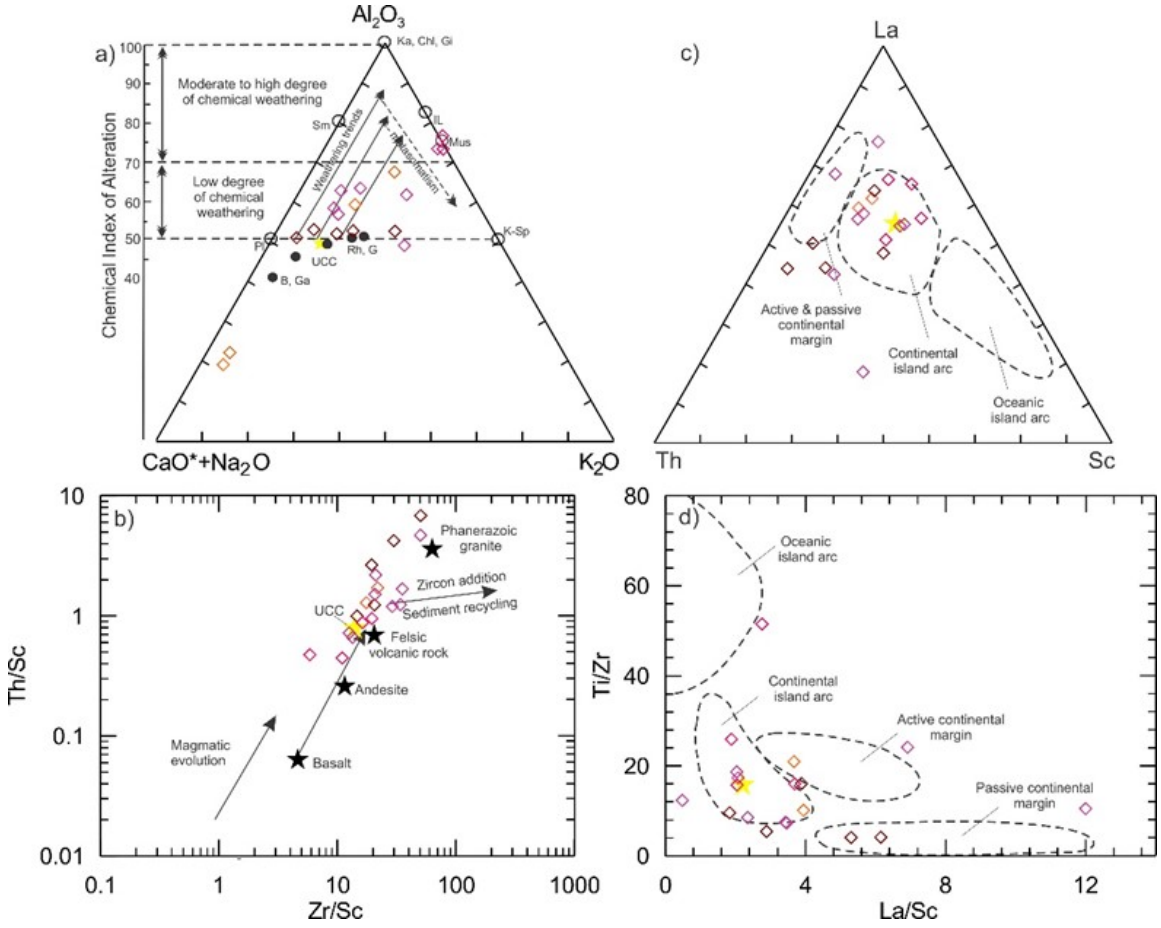

Fig. 13. a) Molecular proportions of the Al_2O_3 – CaO* + Na_2O – K_2O (A-CN-K) ternary diagram (Nesbitt and Young), b) Th/Sc versus Zr/Sc (McLennan, 1989), c, d) La–Th–Sc and Ti/Zr vs La/Sc (Bhatia and Crook, 1986) diagrams for the studied Early and Middle Permian black schist, gneiss and psammitic schists.

granite trend, suggesting that the Middle Permian schists were derived from a source dominated by felsic igneous rocks (Fig. 13a). However, Early Permian black schist plotted within the 'Muscovite' region, an indication of high weathering at the source. Thus, Middle Permian psammitic schist represent mainly immature deposits, while Early Permian black schist represent more mature source. From the high alteration indexes, it can be inferred that black schist from the Mogoitiin Gol area are geochemically and texturally mature. In addition, relatively high Rb/Sr ratios of the Early Permian black schist (average 7.7) indicate strong weathering and sedimentary recycling, because weathering and diagenetic processes can lead to a significant increase in Rb/Sr ratios (McLennan et al., 1993). In contrast, the relatively low Rb/Sr ratios of Middle Permian gneiss, psammitic schist and metasandstone (mean 0.81) suggest simple recycling process for such sediments. Also, the

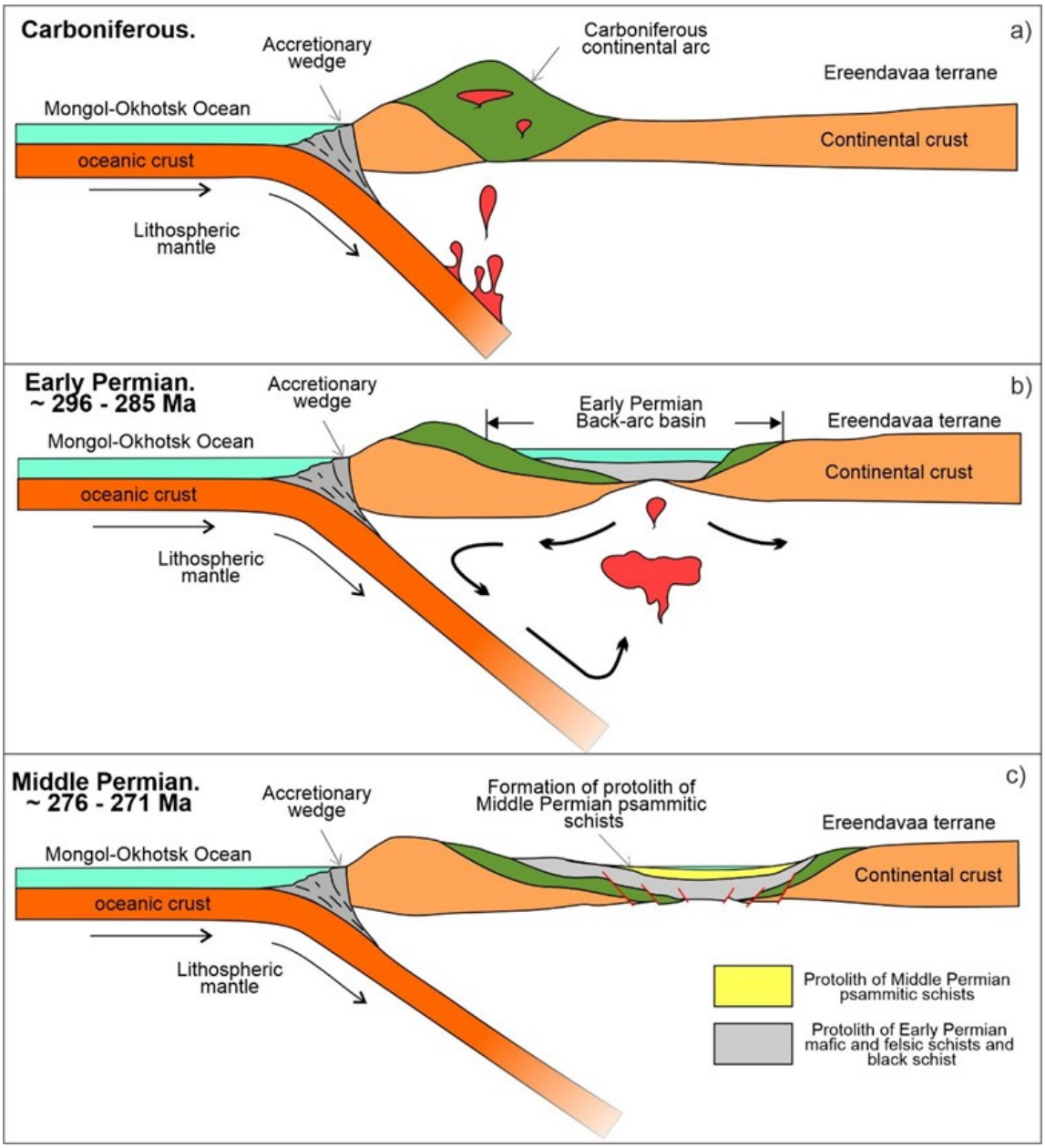

Fig. 14. Simplified scheme showing a geodynamic evolution model for the Ereendavaa terrane, Eastern Mongolia during the Early-Middle Permian.

Th/Sc ratios was used for provenance study, because Th is enriched in silicic rocks, while Sc is more enriched in basic rocks, and the ratio does not vary significant during sedimentary recycling (McLennan et al., 1993; Cullers, 1994). In contrast, Zr/Sc ratio will increase significantly during sediment recycling with zircon enrichment, and can be considered as a useful indicator of heavy mineral concentration (McLennan, 1989).

In this respect, the Early and Middle Permian gneiss and schists show variable Th/Sc (0.43 – 6.85) and Zr/Sc (5.32 – 50.5) values, and form a good positive correlation on the Th/Sc vs Zr/Sc diagram, indicating that the provenance was dominated by felsic source rocks rather than sediment recycling with zircon enrichment (Fig. 13b). This point is supported by the LREE enrichment and strong negative Eu-anomalies (Eu/Eu* = 0.29 – 0.86) in the chondrite-normalized REE pattern of these samples (Fig. 11a), reflecting their derivation from materials having feldspar fractionation and suggesting a provenance dominated by felsic magmatic rocks.

The Early and Middle Permian black schist and gneiss, psammitic schists have geochemical signatures of island arc rocks, such as enrichment of LILE relative to HFSE, and markedly negative Nb, Ta and Ti anomalies (Fig. 11b). They plot in the continental arc field, in the La–Th–Sc (Bhatia and Crook, 1986) and Ti/Zr vs La/Sc diagrams, suggesting that they were formed in a continental arc environment (Fig. 13c and d). Only few samples plotting near the active continental margin field. In addition, based on the detrital zircon population, the source area of the Early Permian schists contained Early Devonian, Early Cambrian rocks, with minor presence of Neoproterozoic materials. In contrast, the source area of the Middle Permian schists is limited and dominated only by Early Permian rocks.

Implications for the Late Paleozoic evolution of the Mongol-Okhotsk Ocean

Based on the above discussion, we propose that the protolith of the Early Permian felsic and mafic schists in the north-eastern part of the Ereendavaa terrane, were formed during a back-arc extension in response to the southward subduction of the Mongol-Okhotsk Oceanic plate (slab).

Recent studies show that the post-collisional extensional tectonic regime was dominated during the Devonian in the Ereendavaa terrane, the southern margin of the Mongol-Okhotsk Ocean (MOO) (Narantsetseg et al., 2019; Miao et al., 2020) and since the Early Carboniferous (ca. 325 Ma), southward subduction of the Mongol-Okhotsk oceanic plate was initiated (Fig. 14a), forming the Adaatsag and Huhu Davaa ophiolites (Tomurtogoo et al., 2005; Zhu et al., 2018). Additionally, magmatic arc zircons recorded in the composition of detrital zircons of the sandstone samples from the Ereendavaa terrane support this point (Bussein et al., 2011).

In the Permian to Triassic, the subduction of the Mongol-Okhotsk oceanic plate was active, to form Andean-type active margin along the both sides of whole Mongol-Okhotsk Belt (MOB) (Badarch et al., 2002; Bussein et al., 2011; Sheldrick et al., 2020). The southern continental arc in the Ereendavaa terrane represented by the Middle Carboniferous – Triassic Middle Gobi volcanic plutonic Belt including Carboniferous to Jurassic granitoids in the Kherlen depression (Bussein et al., 2011). According to this scenario, we propose that accompanied with the emplacement with the arc magmatic rocks, the arc rifting occurred and formed the Early Permian bimodal volcanic rocks, a protolith of the mafic and felsic schists from the north-eastern part of the Ereendavaa terrane (Fig. 14b).

The black schist which recorded in the schists sequence may represent finer silty sediments of the back-arc basin. Also, the high concentration of the U, As and Sb suggest that these elements were accumulated from seawater on oxygen-poor environment or by significant hydrothermal activity.

In addition, published data indicate that the dated Lower Permian mylonitic granites, augen gneiss, gabbro-amphibolite (296 ± 5 to 289 ± 5 Ma, Miao et a, 2017) and orthogneises (283 ± 5 Ma and 282 ± 7 Ma, Dauodene et al., 2013) from the Ereendavaa terrane are mainly felsic and mafic in composition, suggesting that these

rocks may belong to the intrusive analogy of the bimodal volcanic association.

In the Late Permian, after the formation of the back-arc basin, deposition of the immature deposits as wacke, arkose and litharenite dominated sediments started. The provenance characteristics indicate that these sedimentary rocks were deposited on a continental arc environment which received detritus from neighboring Early Permian felsic magmatic rocks (Fig. 14c). In the Triassic, a southward subduction of the Mongol-Okhotsk slab underwent partial melting during the closure of the Mongol-Okhotsk Ocean, forming a high-Si adakite (Sheldrick et al., 2020). Later, during Late Jurassic to Early Cretaceous, the region was affected by a large-scale NW–SE extensional tectonic event with formation of Ereendavaa metamorphic core complex (Daoudene et al., 2009; 2013).

CONCLUSIONS

Based on new geochronological and geochemical analysis of the studied metamorphic rocks, we can draw the following conclusions:

- New LA–ICP–MS zircon U–Pb dating results indicate that the protolith of the metamorphic rocks from the north-eastern part of the Ereendavaa terrane were formed in two stages: 1) ~ 296 - 285 Ma, forming of protoliths of mafic, felsic and black schists, which were previously believed to be Mesoproterozoic or Neoproterozoic in age; 2) ~276 - 271 Ma, deposition of protolith of gneiss and psammitic schists, which were believed before to be Paleoproterozoic and Mesoproterozoic in age.
- The Early Permian bimodal association with low-K basalt and comagmatic high-Na, low-K dacites together with high-K calc-alkaline rhyolites, a protolith of the mafic and felsic schists were formed in a back-arc environment as a result of southward subduction of the Mongol-Okhotsk oceanic plate beneath the Ereendavaa terrane and probably related to the roll-back of the subducted slab.
- The Early Permian black schist and Middle Permian gneiss, psammitic schists have geochemical signatures of island arc rocks, such as enrichment of LILE relative to HFSE, and markedly negative Nb, Ta and Ti anomalies, suggesting that they were formed in a continental arc environment. The source area of the Early Permian schists contained Early Devonian, and Early Cambrian rocks, with minor presence of Neoproterozoic materials. In contrast, the source area of the Middle Permian schists is limited and dominated by only Early Permian rocks.
- We conclude that accompanied with the emplacement with the arc magmatic rocks in the north-eastern part of the Ereendavaa terrane, the arc rifting was occurred and formed the Early Permian bimodal volcanic rocks and Late Permian immature deposits, all which probably metamorphosed during the later Mesozoic magmatic activity.

ACKNOWLEDGEMENTS

The authors would like to express their cordial thanks to the staff of the State Key Laboratory of Isotope Geochemistry, Guangzhou Institute of Geochemistry, CAS and Institute of Geology, CAGS for their advice and assistance during U-Pb dating and geochemical analysis. We are grateful to D. Munkhjin and B. Enkhdalai for their help with the graphical materials. We give our special thanks to the three anonymous reviewers, whose insightful and constructive reviews have greatly improved the paper.

This work was financially supported by the research grant of the Chinese Academy of Sciences President's International Fellowship Initiative program for visiting scientists (2017VCA0010), International Partnership Program of CAS (132744KYSB20190039) as well as the Major State Basic Research Program of the P.R. China (2013CB429803) and the project of 'The basement and cover complexes of the Khatanbulag and South Gobi Massifs: Geology and mineralization of Kherlen-Onon Zone' implemented at Instituite of Geology, Mongolian Academy of Sciences. This paper is also a contribution to IGCP - Project 662 'Orogenic architecture and crustal growth from accretion to collision'.

REFERENCES

Badarch, G., Cunningham, D.W., Windley, B.F. 2002. A new terrane subdivision for Mongolia: Implications for the Phanerozoic crustal growth of Central Asia, Journal of Asian Earth Sciences, v. 21, p. 87-110. https://doi.org/10.1016/S1367-9120(02)00017-2

Barker, F. 1979. Trondhjemite: Differentiation, environment and hypotheses of origin. In: F. Barker (Ed), Trondhjemites, Dacites, and Related Rocks (Developments in Petrology 6), Elsevier. Amsterdam, p. 1-12. https://doi.org/10.1016/B978-0-444-41765-7.50006-X

Byamba, J. 1991. Tectonic evolution of Mongolia in Late Proterozoic-Early Paleozoic, Dr.Sc thesis, Geological Institute, Russian Academy of Sciences, Moscow, 350 p (in Russian).

Bhatia, M.R., Crook, K.A.W. 1986. Trace element characteristics of graywackes and tectonic setting discrimination of sedimentary basins. Contributions to Mineralogy and Petrology, v. 92, p. 181-193. https://doi.org/10.1007/BF00375292

Blagonravov, B.I., Goldenberg, V.I., Blagonravova, L.A., Kazakevich, A.S., Kantorovich, B.I., Korobov, G.S., Krasilnikov, G.M., Pugacheva I.P., Terekhov, A.F., Fedorova, M.I., Chekhovich, M.B. 1990. Report of 1:200000 scale geological mapping, State Geological Fund of Mineral Resources and Petroleum Authority of Mongolia, No 1757, Ulaanbaatar (in Russian).

Bussien, D., Gombojav, N., Winkler, W., Quadt. A. 2011. The Mongol-Okhotsk belt in Mongolia-An appraisal of the geodynamic development by the study of sandstone provenance and detrital zircons. Tectonophysics, v. 510, p. 132-150. https://doi.org/10.1016/j.tecto.2011.06.024

Cabanis, B., Lecolle, M. 1989. Le diagramme La/10-Y/15-Nb/8: un outfil pour la discrimination de seriesvolcaniques et la mise en evidence des processus de mélangeet/ou de contamination crustale. C.R. Acad. Sci. (Ser. II) 309, p. 2023-2029.

Cox, R., Lowe, D.R., Cullers, R.L. 1995. The influence of sediment recycling and basement composition on evolution of mudrock chemistry in the southwestern United States. Geochimica et Cosmochimica Acta, v, 59, p. 2919-2940. https://doi.org/10.1016/0016-7037(95)00185-9

Crawford, A.J., Greene, H.G., Exon, N.F. 1988. Geology, petrology and geochemistry of submarine volcanoes around Epi island. New Hebrides island arc. In: H.G. Greene and F.L. Wong (Eds), Gcology and Offshore Resources of Pacific Island Arcs-Vanuatu Region. Circum-Pacific Council Energy and Mineral Resources. Earth Science Series, v. 8, p. 301-327.

Cullers, R.L. 1994. The geochemical signatures of source rocks in size fractions of Holocene stream sediment derived from metamorphic rocks in the Wet Mountains region, USA. Chemical Geology, v. 113, p. 327-343. https://doi.org/10.1016/0009-2541(94)90074-4

Daoudene, Y., Gapais, D., Ledru, P., Cocherie, A., Hocquet, S., Donskaya, T.V. 2009. The Ereendavaa Range (north-eastern Mongolia): an additional argument for Mesozoic extension. International Journal of Earth Science, v. 98(6), p. 1381-1393. https://doi.org/10.1007/s00531-008-0412-2

Daoudene, Y., Gilles, R., Alain, C., Patrick, L., Denis, G. 2013. Timing of exhumation of the Ereendavaa metamorphic core complex (north -eastern Mongolia) - U-Pb and 40Ar/39Ar constraints, Journal of Asian Earth Sciences, v. 62, p. 98-116. https://doi.org/10.1016/j.jseaes.2011.04.009

Dash, B., Yin, A., Jiang, N., Tseveendorj, B., Han B. 2015. Petrology, structural setting, timing, and geochemistry of Cretaceous volcanic rocks in eastern Mongolia: Constraints on their tectonic origin, Gondwana Research, v. 27. p. 281-299. https://doi.org/10.1016/j.gr.2013.10.001

Dilek, Y., Harald, F. 2011. Ophiolite genesis and global tectonics: Geochemical and tectonic fingerprinting of ancient oceanic lithosphere, GSA Bulletin v. 123(3-4), p. 387-411. https://doi.org/10.1130/B30446.1

Dorjnamjaa, D., Bat-Ireedui, Ya, 1991. Precambrian of Mongolia, 182 p (in Russian).

Dorjnamjaa, D., Byamba, J., Enkhbaatar, B., 2012. Precambrian of Mongolia, in: Geology and mineral resources of Mongolia, v. 1, Stratigraphy, 54-81 (in Mongolian).

Erdenechimeg, D., Enkhbayar, B., Boldbaatar, G., Damdinjav, B., Taivanbaatar, Ts. 2017.

Report of the project of compilation of the 1:500000 scale Geological Map of Mongolia State Geological Fund of Mineral Resources and Petroleum Authority of Mongolia, No 8480, Ulaanbaatar

Gale, A., Dalton C.A., Langmuir Ch.H., Su, Yo., Schilling, J.G. 2013. The mean composition of ocean ridge basalts, Geochemistry, Geophysics, Geosystems, v. 14(3), p. 489-518. https://doi.org/10.1029/2012GC004334

Herron, M.M. 1988. Geochemical classification of terrigenous sands and shales from core or log data, Journal of Sedimentary Research, v. 58(5), p. 820-829. https://doi.org/10.1306/212F8E77-2B24-11D7-8648000102C1865D

Hochstaedter, A., Gill, J., Peters, R., Broughton, P., Holden, P., Taylor, B. 2001. Across-arc geochemical trends in the Izu-Bonin arc: Contributions from the subducting slab, Geochemistry, Geophysics, Geosystems, v. 2, https://doi.org/10.1029/2000GC000105

Jahn, B.M. 2004. The central Asian Orogenic Belt evolution and growth of the continental crust in the Phanerozoic. In: Malpas, J., Fletcher, C.J.N., Ali, J.R., Aichison, J.C. (Eds.), Aspects of the Tectonic Evolution of China. Geological Society, London, Special Publications 226, p. 73-100. https://doi.org/10.1144/GSL.SP.2004.226.01.05

Khain, E.V., Bibikova, E.V., Salnikova, E.B., Kroner, A., Gibsher, A.S., Didenko, A.N., Degtyarev, K.E., Fedotova, A.A. 2003. The Paleo-Asian Ocean in the Neoproterozoic and early Paleozoic: New geochronological data and palaeotectonic reconstructions. Precambrian Research, v. 122, p. 329-358. https://doi.org/10.1016/S0301-9268(02)00218-8

Koschek, G., 1993. Origin and significance of the SEM cathodoluminescence from zircon, Journal of Microscopy, v. 171(3), p. 223-232. https://doi.org/10.1111/j.1365-2818.1993.tb03379.x

Kotov, A.B., Mazukabzov, A.M., Skovitina, T.M., Sorokin, A.P., Velikoslavinskii, S.D., Sorokin, A.A., 2013. Structural evolution of the Gonzha Block (Argun-Idermeg superterrane of the Central Asian Orogenic Belt), Doklady Earth Sciences, v. 448 (2), p. 168-171. https://doi.org/10.1134/S1028334X1302013X

Langmuir C.H., Bezos A., Escrig S., Parman S, 2006. Chemical Systematics and Hydrous Melting of the Mantle in Back-Arc Basins. Geophysical Monograph Series 166, p. 87-146. https://doi.org/10.1029/166GM07

Liu, Y.S., Gao, S., Hu, Z.C., Gao, G.C., Zong, K.Q., Wang, D.B., 2010. Continental and oceanic crust recycling-induced melt-peridotite interactions in the Trans-North China Orogen: U-Pb dating, Hf isotopes and trace elements in zircons from mantle xenoliths. Journal of Petrology, v. 51(1-2), p. 537-571. https://doi.org/10.1093/petrology/egp082

Le Maitre, R.W. 1989. A classification of igneous rocks and glossary terms, recommendations of the International Union of Geological Sciences Subcommission on the Systematics of Igneous Rocks. Blackwell Scientific Publications, Oxford, p. 1-193

Long, X., Yuan, Ch., Sun, M., Zhao, G., Xiao, W., Wang, Y., Yang, Y., Hu, A. 2010. Archean crustal evolution of the northern Tarim craton, NW China: Zircon U-Pb and Hf isotopic constraints. Precambrian Research, v. 180, p. 272-284. https://doi.org/10.1016/j.precamres.2010.05.001

Ludwig, K.R. 2003. Isoplot/Ex, Version 3: a geochronology Toolkit for Microsoft Excel. Berkeley Geochronology Center, Special Publication 4, p. 1-70.

Marinov, N.A., Zonenshain, L.P., Blagonravov, V.A. (Eds.), 1973. Geology of the Mongolian People's Republic, v. 1, Stratigraphy, Nedra, Moscow, 782 p (in Russian).

McLennan, S.M. 1989. Rare earth elements in sedimentary rocks: Influence of provenance and sedimentary processes. Reviews in Mineralogy and Geochemistry, v. 21, p. 169-200. https://doi.org/10.1515/9781501509032-010

McLennan, S.M., Hemming, S., McDaniel, D.K., Hanson, G.N. 1993. Geochemical approaches to sedimentation, provenance, and tectonics. Geological Society of America Special Paper 284, p. 21-40. https://doi.org/10.1130/SPE284-p21

Miao, L, C., Zhang, F.Q., Baatar, M., Zhu, M.S., Anaad, C. 2017. SHRIMP zircon U-Pb ages and tectonic implications of igneous events in

the Ereendavaa metamorphic terrane in NE Mongolia. Journal of Asian Earth Science. v. 144, p. 243-260. https://doi.org/10.1016/j.jseaes.2017.03.005

Miao, L.C., Baatar, M., Zhang, F.Q., Anaad, C., Zhu, M.S., Yang, S.H. 2016. Cambrian Kherlen ophiolite in northeastern Mongolia and its tectonic implications: SHRIMP zircon dating and geochemical constraints. Lithos, v. 261, p. 128-143. https://doi.org/10.1016/j.lithos.2015.12.012

Miao, L.C., Zhu, M., Liu, Ch., Baatar, M., Anaad, C., Yang S.H., Li,X. 2020. Detrital-Zircon Age Spectra of Neoproterozoic-Paleozoic Sedimentary Rocks from the Ereendavaa Terrane in NE Mongolia: Implications for the Early-Stage Evolution of the Ereendavaa Terrane and the Mongol-Okhotsk Ocean, Minerals, v. 10, p. 1-23. https://doi.org/10.3390/min10090742

Mossakovsky, A.A., Ruzhentsev, S.V., Samygin, S.G., Kheraskova, TN. 1994. Central Asian fold belt: Geodynamic evolution and formation history, Geotectonics, v. 27, p. 445-474.

Nakada, S., Maillet, P., Monjaret, M.C., Fujinawa, A., Urabe, T. 1994. High-Na dacite from the Jean Charcot Trough (Vanuatu), Southwest Pacific, Marine Geology, v. 116, p. 197-213. https://doi.org/10.1016/0025-3227(94)90176-7

Narantsetseg, Ts., Yuan, Ch., Tomurhuu, D., Delgerzaya, P., Enkh-Orshikh, O. 2015. Problems of geochronology, geochemistry and geodynamic condition of metamorphic complexes of Herlen area, The Explorer, v. 53, p. 69-88 (in Mongolian).

Narantsetseg, Ts., Yuan, Ch., Ren, Zh., Orolmaa, D., Baatarchuluun, O., Tumendelger, J., Battushig, A. 2019. U-Pb detrital zircon dating of metamorphic rocks in Ereendavaa terrane, NE Mongolia: timing of formation and metamorphism. Abstract volume of project IGCP-662, Orogenic architecture and crustal growth from accretion to collision, 15-22 September, 2018, China

Narantsetseg, Ts., Orolmaa, D., Yuan, Ch.,

Wang, T., Guo, L., Tong, Y., Wang, X., Enkh-Orshikh, O., Oyunchimeg, Ts.; Delgerzaya, P., Early-Middle Paleozoic volcanic rocks from the Ereendavaa terrane (Tsarigiin gol area, NE Mongolia) with implications for tectonic evolution of the Kherlen massif. Jornal of Asian Earth Science, v. 175, p. 138-157. https://doi.org/10.1016/j.jseaes.2018.12.008

Nesbitt, H.W., Young, G.M. 1982. Early Proterozoic climates and plate motions inferred from major element chemistry of lutites, Nature, v. 199, p. 715-717. https://doi.org/10.1038/299715a0

Parfenov, L. M., Badarch, G., Berzin, N. A., Khanchuk, A. I., Kuzmin, M. I., Nokleberg, W. J., Prokopiev, A. V., Ogasawara, M., Yan, H. 2009. Summary of Northeast Asia geodynamics and tectonics, Stephan Mueller Special Publication Series 4, p. 11-33. https://doi.org/10.5194/smsps-4-11-2009

Pearce, J.A., Stern, R.J., Bloomer, Sh.H., Fryer, P. 2005. Geochemical mapping of the Mariana arc-basin system: Implications for the nature and distribution of subduction component, Geochemistry, Geophysics, Geosystems, v. 6(7), Q07006. https://doi.org/10.1029/2004GC000895

Pearce, J.A., Stern, R.J. 2006. Origin of Back-Arc Basin Magmas: Trace Element and Isotope Perspectives, Back-Arc Spreading Systems: Geological, Biological, Chemical, and Physical Interactions Geophysical Monograph Series 166, p. 63-86. https://doi.org/10.1029/166GM06

Pearce, J.A., Harris, N.B.W., Tindle, A.G. 1984. Trace element discrimination diagrams for the tectonic interpretation of granitic rocks. Journal of Petrology, v. 25, p. 115-125. https://doi.org/10.1093/petrology/25.4.956

Ross P.S., Bédard J.H. 2009. Magmatic affinity of modern and ancient subalkaline volcanic rocks determined from trace-element discriminant diagrams, Canadian Journal of Earth Sciences, v 46(11), https://doi.org/10.1139/E09-054

Saccani, E. 2015. A new method of discriminating different types of post-Archean ophiolitic basalts and their tectonic significance using Th-Nb and Ce-Dy-Yb systematics, Geoscience Frontiers, v. 6, p. 481-501. https://doi.org/10.1016/j.gsf.2014.03.006

Sengör, A.M.C., Natal'in, B.A., Burtman, V.S., 1993. Evolution of the Altaid tectonic collage and Palaeozoic crustal growth in Eurasia.

Nature, v. 364, p. 299-306. https://doi.org/10.1038/364299a0

Sengör, A.M.C., Natal'in, B.A., 1996. Paleotectonics of Asia: fragments of synthesis. In: Yin, A., Harrison, T.M. (Eds.). The Tectonic Evolution of Asia. Cambridge University Press, p. 486-640.

Sheldrick, T.C., Barry, T.L., Millar, L.L., Barfod, D.N., Halton, A.M., Smith, D.J. 2020. Evidence for southward subduction of the Mongol-Okhotsk oceanic plate: Implications from Mesozoic adakitic lavas from Mongolia, Gondwana Research, v. 79, p. 140-156. https://doi.org/10.1016/j.gr.2019.09.007

Sun, S.S., McDonough, W.F., 1989. Chemical and isotopic systematic of oceanic basalts: implications for mantle composition and processes. In: Saunders, A.D., Norry, M.J. (Eds.), Magmatism in the Oceanic Basins, v. 42. Geological Society of London, p. 313-345. https://doi.org/10.1144/GSL.SP.1989.042.01.19

Taylor, B., Martinez, F. 2003. Back-arc basin basalt systematics, Earth and Planetary Science Letters, v. 210 (3-4), p. 481-497. https://doi.org/10.1016/S0012-821X(03)00167-5

Taylor, S.R., McLennan, S.M. 1985. The continental crust: its composition and evolution. Blackwell Scientific Publications, Oxford, UK, p. 312.

Tomurtogoo, O., Windley, B.F., Kröner, A., Badarch, G., Liu, D.Y. 2005. Zircon age and occurrence of the Adaatsag ophiolite and Muron shear zone, Central Mongolia: Constraints on the evolution of the Mongol-Okhotsk ocean, suture and orogen. Journal of the Geological Society of London, v. 162, p. 125-134. https://doi.org/10.1144/0016-764903-146

Tomurtogoo, O. 2002. Brief Explanatory Notes to the Tectonic Map of Mongolia at the scale of 1:1,000,000. Mineral Resources Authority of Mongolia.

Tomurtogoo, O. 2012. Tectonic subdivision of orogenic Belt of Mongolia, Geology 21, Transactions of Institute of Geology and Mineral Resources of MAS, 5-25 (in Mongolian).

Tomurtogoo, O., 2014. Tectonics of Mongolia, in: Tectonics of Northern, Central and Eastern Asia, explanatory note to the Tectonic map of Northern Central Eastern Asia and adjacent areas at scale 1:2500000, p. 110-126.

Wang, T., Guo, L., Zhang, L., Yang, Q., Zhang, J., Tong, Y., Ye, K. 2015. Timing and evolution of Jurassic-Cretaceous granitoid magmatisms in the Mongol-Okhotsk belt and adjacent areas, NE Asia: Implications for transition from contractional crustal thickening to extensional thinning and geodynamic settings, Journal of Asian Earth Sciences, v. 97, p. 365-392. https://doi.org/10.1016/j.jseaes.2014.10.005

Wang, T., Tong, Y., Zhang, L., Li, S., Huang H., Zhang, J., Guo, L., Yang, Q., Hong, D., Donskaya, T., Gladkochub, D., Narantsetseg, Ts. 2017. Granitoids in the middle and eastern parts of Central Asian and their tectonic significance, Journal of Asian Earth Sciences, v. 145, p. 368-392. https://doi.org/10.1016/j.jseaes.2017.06.029

Winchester J.A., Floyd P.A. 1977. Geochemical discrimination of different magma series and their differentiation products using immobile elements, Chemical Geology, v. 20, p. 325-343. https://doi.org/10.1016/0009-2541(77)90057-2

Windley, B. F., Alexeiev, D., Xiao, W., Kroner, A., and Badarch, G. 2007. Tectonic models for accretion of the Central Asian Orogenic Belt. Journal of the Geological Society of USA, v. 164 (12), p. 31-47. https://doi.org/10.1144/0016-76492006-022

Wood, D.A. 1980. The application of a Th-Hf-Ta diagram to problems of tectonomagmatic classification and to establishing the nature of crustal contamination of basaltic lavas of the British Tertiary volcanic province, Earth and Planetary Science Letters, v. 50, p. 11-30. https://doi.org/10.1016/0012-821X(80)90116-8

Xiao, W.J., Huang, B.C., Han, C.M., Sun, S., Li, J.L. 2010. A review of the western part of the Altaids: a key to understanding the architecture of accretionary orogens. Gondwana Research, v. 18, p. 253-273. https://doi.org/10.1016/j.gr.2010.01.007

Xiao, W., Windley, B.F., Han, H., Liu, W., Wan, B., Zhang, J., Ao, S., Zhang, Z., Song, D. 2018. Late Paleozoic to early Triassic multiple roll-back and oroclinal bending of the Mongolia collage in central Asian Earth Science Reviews, v. 186, p. 94-128.

https://doi.org/10.1016/j.earscirev.2017.09.020

Yuan, C., Sun, M., Wilde, S., Xiao, W.J., Xu, Y.G., Long, X.P., Zhao, G.C. 2010. Postcollisional plutons in the Balikun area, East Chinese Tianshan: evolving magmatism in response to extension and slab break-off. Lithos, v. 119, p. 269-288. https://doi.org/10.1016/j.lithos.2010.07.004

Zhu, M., Zhang, F., Miao, L., Baatar, M., Anaad, C., Yang, S., Li, X. 201. The late Carboniferous Khuhu davaa ophiolite in northeastern Mongolia: Implications for the tectonic evolution of the Mongol-Okhotsk ocean. Geological Journal, v. 53, p. 1263-1278. https://doi.org/10.1002/gj.2955

Zorin, Yu. A., 1999. Geodynamics of the western part of the Mongolia-Okhotsk collisional belt, Trans-Baikal region (Russia) and Mongolia. Tectonophysics, v. 306, p. 33-56. https://doi.org/10.1016/S0040-1951(99)00042-6